Simple Power Transformer Fiber Bragg Grating Temperature Sensor

Faezeh Mobasheri

A Thesis

In

The Department

of

Electrical and Computer Engineering

Presented in Partial Fulfillment of Requirements

For the Degree of Master of Applied Science

(Electrical & Computer Engineering) at

Concordia University

Montreal, Quebec, Canada

September 2016

© Faezeh Mobasheri, 2016

CONCORDIA UNIVERSITY

School of Graduate Studies

This is to certify that the thesis prepared

By: Faezeh Mobasheri

Entitled: Simple Power Transformer Fiber Bragg Grating Temperature Sensor

and submitted in partial fulfillment of the requirements for the degree of

Master of Applied Science

Complies with the regulations of this University and meets the accepted standards with respect to originality and quality.

Signed by the final Examining Committee:

_____Chair

Dr. R. Raut

_____Internal Examiner

Dr. X. Zhang

_____External Examiner

Dr. A. Dolatabadi

_____Supervisors

Dr. M. Kahrizi

Approved_____

Chair of Department of Graduate Program Director

_____2016_____

Abstract

Simple Power Transformer Fiber Bragg Grating Temperature Sensor

Faezeh Mobasheri

This study has designed, developed, and tested a high temperature sensor based on Fiber Bragg grating. The new introduced interrogation system makes the sensor suitable for installation inside the power transformer. Unlike the existing fiber Bragg grating based temperature sensors, the interrogation system of the sensor is based on amplitude modulation (AM). The distinctive characteristics of the designed temperature sensor, in addition to inherent advantages of FBG is, its real-time monitoring, small size, and low cost. The sensor is tested in harsh environment at temperature starting from -27 ºC to 400 ºC. The long-term stability and reliability of the designed sensors of one sensor head is tested in furnace at 400 ºC for 338 hours. Furthermore, the sensor head was under test in 600 ºC for about 18 hours. The sensor head which is used in this experiment is fiber Bragg grating Corning SMF-28, Ge-doped optical fibers with 4% Ge content in its core. It was loaded with hydrogen prior to writing with 248 nm excimer laser. The Bragg wavelength of the two prepared sensors head for this work is around 1530 nm and 1550 nm.

In this study, we used Amplified spontaneous emission (ASE) light source as an input light for the sensor head. ASE light source makes it possible to have linear input light in two different ranges with 4 nm span. The sensors head Bragg wavelength is designed in the range in which the ASE light source spectrum is linear. The sensor has the Photodiode (PD) to convert the Bragg reflected spectrum power into its equivalent current.

Acknowledgements

I would like to express my gratitude to my supervisor, Dr. Mojtaba Kahrizi, whose expertise, understanding, and patience, added considerably to my graduate experience. I appreciate his vast knowledge and skill in many areas, and his assistance in writing reports and thesis. I would like to thank the other members of this study, Dr. Bowei Zhang for the assistance he provided at all levels of the research project.

I also want to thank all my examination committee members for their time and their wonderful comments on my work.

I must express my very profound gratitude to my family for the support they provided me through my entire life and in particular, I must acknowledge my husband and best friend, Hossein, without whose love, encouragement and editing assistance, This accomplishment would not have been possible.

Contents

List of figures vii

List of tables x

list of abbreviations xi

1 Introduction 1

1.1 Research objective 4

1.2 Chapters overview 5

2 Introduction to Fiber Bragg gratings 6

2.1 Properties of Fiber Bragg gratings 8

2.1.1 Uniform Bragg Grating Reflectivity 10

2.2 Classification of fiber Bragg grating 13

2.3 Methods for fiber Bragg grating fabrication 14

2.3.1 Phase-mask technique 15

2.4 Photosensitivity of Fibers 17

2.4.1 History of photosensitivity 17

2.4.2 Defects in germanosilicate optical fiber 21

2.5 Photosensitization Techniques of Fiber Bragg Grating 25

3 System design 28

3.1 Designed temperature sensor 31

4 Amplified Spontaneous Emission Light Source 35

4.1 Principle of ASE Light Source 35

4.2 ASE light source spectrum analysis 38

5 The Bragg Wavelength Analysis and Long Term Stability Testing 43

5.1 Initial Data of the Sensor Head 44

5.2 Optical Spectrum Analyzer Calibration 48

5.3 Sensor Calibration 52
5.4 Long-term Stability Testing 57
6 Conclusion, contributions and future works 62
6.1 Summary of Thesis 62
6.2 Suggestion for Future Work 63
7 References 64

List of figures

Figure 1-1 The explosion inside the power transformer plant [4]. 2
Figure 2-1 The cross section of typical single-mode telecommunication optical fiber with the refractive index profile. 6
Figure 2-2 Uniform Bragg grating [12] 9
Figure 2-3 Refractive index modulation and effective refractive index of the grating structure [13]. 11
Figure 2-4 Simulation of the reflection spectra of a 10 mm long uniform grating as a function of wavelength ($\Delta n = 1*10\text{-}4$)[13]. 12
Figure 2-5 Types of fiber gratings. (a) Fiber Bragg grating, (b) long-period fiber grating, chirped fiber grating, (d) tilted fiber grating, (e) sampled fiber grating [9]. 14
Figure 2-6 Schematic of the phase-mask fabrication method [17]. 16
Figure 2-7 Interference pattern of the phase-mask writing method [18]. 17
Figure 2-8 CW distributed feedback argon ion laser. The fiber reflection filter (~1m long) takes the place of output reflector and gives rise to narrow band oscillation [23]. 19
Figure 2-9 oxygen deficient germania defects thought to be responsible for the photosensitive effect in germania-doped silica. An electron is released on breaking of the bond [11]. 20
Figure 2-10 Transmission loss spectrum of a 15 um which is shown before and after UV radiation at 244 nm[26]. 21
Figure 2-11 Common point defects of germanosilicate thought to be responsible for photosensitivity. GODCs (left) which are believed to absorb around 244 nm and produce the GeE' defect and liberate electrons which are captured to form Ge(1) and Ge(2) sites (right)[7]. 23
Figure 2-12 The germania-doped silica fiber GeO defects, in which the germanium atom bonds with either silicon or germanium. If the defect absorbs a photon it can form a GeÉ' defect. The GeÉ' center is Ge(0) or Ge(3). The GeÉ' has an extra electron (associated with the Ge atom) which is free to move in glass matrix until it traps at original defect site, at hole site of another GeÉ', or at any of the Ge(n) defects [7]. 24
Figure 2-13 Absorption at 242 nm in perform samples before and after collapse as a function of Ge concentration [29]. 26
Figure 3-1 schematic of the interrogation system using OSA. 29

Figure 3-2 schematic of an experimetal setup without using OSA [33]. 31
Figure 3-3 Configuartion of the designed high temperature sensor based on fiber Bragg grating. 32
Figure 3-4 The ASE light sorce output spctrum. 33
Figure 3-5 Working principle of the sensor followed by an interrogation system. 34
Figure 4-1 Amplified spontanneous emissionn spectrum. 35
Figure 4-2 the rare earth ions can emit the light at different wavelength from the pump light [36]. 36
Figure 4-3 Three different process during the interaction of light with matter [35]. 36
Figure 4-4 The spontaneous emission is amplified by stimulated emission as the light passes through the fiber core [36]. 37
Figure 4-5 the analysis of the ASE light source spctrum. 40
Figure 4-6 The analysis of the ASE light source spctrum. 41
Figure 4-7 42
Figure 5-1 a) The prepared sensor head with Bragg grating at 1549.7 nm. b) The system configuration for FBG testing. 45
Figure 5-2 The return signal of the FBG sensor head with Bragg wavelength at 1549.7 nm at room temperature. 46
Figure 5-3 The return signal of the FBG sensor head with Bragg wavelength at 1549.7 nm at 0°C. 46
Figure 5-4 Fiber Bragg grating backward reflected light with the Bragg wavelenngth at 1529.55 nm at room tempearture. 47
Figure 5-5 The return signal of the FBG with Bragg wavelength at 1529.55 nm at 0 °C. 47
Figure 5-6 screenshot of the OSA setting during the experiment. 49
Figure 5-7 The reflected spectrum of the FBG with the Bragg wavelength at 1529.55 nm at room temperature. The wavelength resolution bandwidth of the OSA is set on 0.1 nm for getting this sepctrum. 50
Figure 5-8 The reflected spectrum of the FBG with the Bragg wavelength at 1529.55 nm at room temperature. The wavelength resolution bandwidth of the OSA is set on 0.5 nm for getting this sepctrum. 51

Figure 5-9 The reflected spectrum of the FBG with the Bragg wavelength at 1529.55 nm at room temperature. The wavelength resolution bandwidth of the OSA is set on 1 nm for getting this sepctrum. 52
Figure 5-10 Change in the Bragg wavelength with respect to running the temperature up to 400°C from 0 °C in expermental result (blue line), and in simulation (orange line)and their fisrt degree regression line. The normalized refraction index change during the running up the temperature (grey line). 54
Figure 5-11 Change in the Bragg wavelength with respect to running the temperature up to 400°C from -27 °C in experimental result (blue line), and in simulation (orange line)and their fisrt degree regression line. The normalized refraction index change during the running up the temperature (grey line). 56
Figure 5-12 The FBG back reflected light at 0°C after 338 hours annealing at 400 °C (blue line) and the FBG back reflected spctrum at 0 °C before annealing (orange line) in sensor head with Bragg wavelength at 1549.7 nm. 59
Figure 5-13 The FBG back reflected light at 0°C after 18 hours annealing at 600°C (blue line) and the FBG back reflected spctrum at 0 °C before annealing (orange line) in sensor head with Bragg wavelength at 1549.7 nm. 60
Figure 5-14 the sensor head reflectivity drift at 600 °C for 2000 seconds with Bragg wavelength at 1549.7 nm..... 61

List of tables

Table 1 Regression table of the data from change in the Bragg wavelength with respect to temperature for sensor head with peak reflection at 1529.55 nm. 55
Table 2 Regression table of the data from change in the Bragg wavelength with respect to temperature for sensor head with peak reflection at 1549.7 nm 57

list of abbreviations

Fiber Bragg grating	FBG
Resistance temperature detector	RTD
Frequency modulation	FM
Optical spectrum analyzer	OSA
Amplitude modulation	AM
Amplified spontaneous modulation	ASE
Wavelength division multiplexer	WDM
Dense wavelength division multiplexer	DWDM
Optical add/drop multiplexer	OADM
Long period grating	LPG
Ultraviolet	UV
Continuous wave	CW
Modified chemical vapor deposition	MCVD
Outside vapor phase deposition	OVPD
Germanium oxygen deficient center	GODC
Neutral oxygen vacancy	NOV
Nonbridging oxygen hole center	NBOHC
Peroxy radical	P-OHC
Electromagnetic interference	EMI
Photodiode	PD
Full width half maximum	FWHM
Bandwidth	BW
Erbium-doped fiber amplifier	EDFA
Light emitting diode	LED
Angled physical contact	APC
Resolution bandwidth	RBW
Analysis of variance	ANOVA
Fourier transform	FFT

1 Introduction

A sensor is an instrument responsible to detect events or changes in its environment, and present the corresponding output. Sensors may provide various types of output, it acts as a transducer, but the output is in the form of electrical or optical signals. The optical fiber senor technology is a direct outgrowth of the revolutions taken place in optoelectronics and fiber optic communication industries[1].

The most commonly used type of all sensors is those which detect temperature or heat. This kind of temperature sensor can vary from the simple one, which controls domestic hot water heating with ON/OFF thermostatic devices to the most complex one with highly sensitive semiconductor types, which can control complex process of control furnace plants. There are many differences between various types of temperature sensors devices.

The remarkable amount of innovation over the past two decades in the optoelectronics and fiber optic communication industries has decreased the prices of optical component and improved the quality. To consider all these economies scale, fiber-optic sensors and related instruments have changed from experimental research applications in the labs to broad usage and applicability in field applications such as structural temperature, strain, and health monitoring. For our research, the fiber-optic sensor utilized for power transformer.

A transformer consists essentially of a magnetic core built up insulated silicon steel lamination upon which are wound two distinct set of coils suitable located with respect to each other and termed the primary and secondary windings. The power transformer is a static machine, used for power transforming from one circuit to another without frequency changing. The transformer named as a static device since it does not have any rotating or moving part. It works on the principle of mutual electromagnetic induction and operates on AC supply[2].

Power transformer includes different parts, such as Core, winding, insulating materials, transformer oil, etc. as an example. Core is responsible for supporting the windings in the transformer. It also provides a low reluctance path to the flow of magnetic flux. There are two windings wound over the transformer core that are insulated from each other. Windings consists of several turns of copper coils bundled together an each bundles are connected in series to form a winding[3].

Figure 1-1 The explosion inside the power transformer plant [4].

Power transformer needs a real time temperature sensor to control its temperature in order to prevent the explosion. The temperature sensor should be immune to electromagnetic interference. In situation in power transformer when the current is increasing, also, the coil temperature is increasing and this high temperature may cause the explosion in the power transformer. Electrically-based temperature sensors, such as thermocouples and Resistance temperature device (RTD) sensor is one of the most famous sensor for measuring temperature of transformer. RTD sensors have their own limitation that promote us to use other kind of the temperature sensors. It

can only install outside of the coil and cannot directly measure the coil temperature[5]. Figure 1-1 is one of the reported explosion in the power transformer plant.

In this work we introduce a high temperature optical sensor. Corresponding simple designed temperature sensor is an apt device for measuring temperature of core and winding inside the power transformer. The design of the sensor is based on Fiber Bragg Grating (FBG) and its application is to measure multi-point sensing.

Some well-known advantages make the FBG interesting as a sensor head for temperature monitoring such as its small size, passive nature, immunity to electromagnetic interference, and capability to measure the physical parameters directly. The other advantage of FBG, which make it desirable for measuring the temperature inside the power transformer, is its capability for real-time temperature monitoring.

Fiber Bragg grating based high temperature sensor is measuring the temperature of the power transformer. If the situation is not under control inside power transformer and caused the winding temperature increases too fast, a real-time high temperature sensor can be used to detect the issue and immediately stop transformer. The other temperature sensors that is developed for measuring the temperature of power transformer can use to measure the cooling temperate.

The existing setup of the FBG temperature sensor work are based on frequency modulation (FM). The system includes light source, FBG, circulator, optical spectrum analyzer (OSA) and PC. The light coupled into the fiber core, part of the light that meet the Bragg condition will then reflect back through the circulator and enter the OSA. In the next step through the OSA, the Bragg wavelength will determine. As the ambient temperature of the FBG sensor head changes, the Bragg wavelength shift toward blue shift or red shift. The relation between the temperature and the shift in the Bragg wavelength is linear, so with measurement of the Bragg wavelength, determination of the temperature is possible.

In this study, the system based on FBG is introduced. The system works based on amplitude modulation (AM) for short distance. The sensor includes amplified spontaneous emission (ASE) broadband light source, two splitters, two photodetectors, optical fiber circulator, FBG at around 1530 nm, and1550 nm Bragg wavelength and OSA for the calibration. The complete system setup has been discuses in chapter four.

Our designed fiber Bragg grating temperature sensor has some advantages over the existing setup of FBG temperature sensors. The FBG system is low power; it means that this sensor can run by battery drives. Only two batteries can supply the power that is needed in this sensor. This sensor can also applied as multi-point temperature sensor just by adding more one-point module/building block and optical switch. The other advantages of this design are that the system has capability of self-calibration, it is reliable, the system is immune to electromagnetic interferences, the system has simple configuration, and it is cost effective.

1.1 Research objective

The objective of this research is to develop a high temperature fiber optic sensor suitable for real-time temperature monitoring inside the core and the winding of the power transformer.

To achieve this objective, the following steps are carried out:

- Literature review regarding fiber Bragg grating and its characteristics.
- Investigation of temperature effect on the fiber Bragg grating.
- Preparing sensor head Based on fiber Bragg grating suitable to use at temperature up to 400ºC.
- Testing the system at high temperature, measuring the shift in the Bragg wavelength with respect to temperature.
- Testing the stability of the sensor head in long-term usage at 400ºC and the higher temperature at 600ºC.

1.2 Chapters overview

First chapter presents an introduction to power transformer Fiber Bragg grating temperature controller. The application of fiber Bragg grating inside the power transformer discussed in this chapter. The condition of using the designed FBG temperature sensor also covered in this chapter. The designed FBG temperature controller introduced and compared with the current setup for FBG temperature sensor.

In second chapter, we discuss some principles regrading FBG. The techniques to write the FBG and the method to increase the photosensitivity introduced in this chapter.

The third chapter is about the system design. In this chapter the pros and cons of the present interrogation system of FBG temperature sensor is presented and in the end of chapter, our new designed temperature sensor is introduced.

In chapter 4, the amplified spontaneous emission (ASE) light source is introduced. The principle of ASE light source and its function also is covered. The ASE light source spectrum analyzed in this chapter.

Chapter 5 allocated to present the characteristics of the designed FBG temperature controller for power transformer application. The principle behind the configuration and the experimental result also mentioned in this chapter. Because the designed sensor system is, based on the Bragg wavelength, so some testing done regrading to confirm the stability of the FBG sensor in our application. The experimental result and simulation of long-term stability at temperature 400^{0}C discussed in this chapter. The effect of increasing and decreasing of temperature investigated in this chapter.

The last chapter covers the conclusion. Suggestion for future work provided in this part of thesis.

2 Introduction to Fiber Bragg gratings

Vast progress on multimedia technologies has come up with active development of many kind of broadband services as an instance, data, video, and voice communication with mean of access network[6]. Different types of optical fiber cable have been researched, developed and partially employed for various applications. The optical fibers have impressive impact on modern telecommunication system. The capacity of optical fiber system is moving forward because of high demand for the internet. By the time pass, the demand for interactive long-distance communication will increase; due to it is needed to reduce energy consumption to prevent the global warming[7].

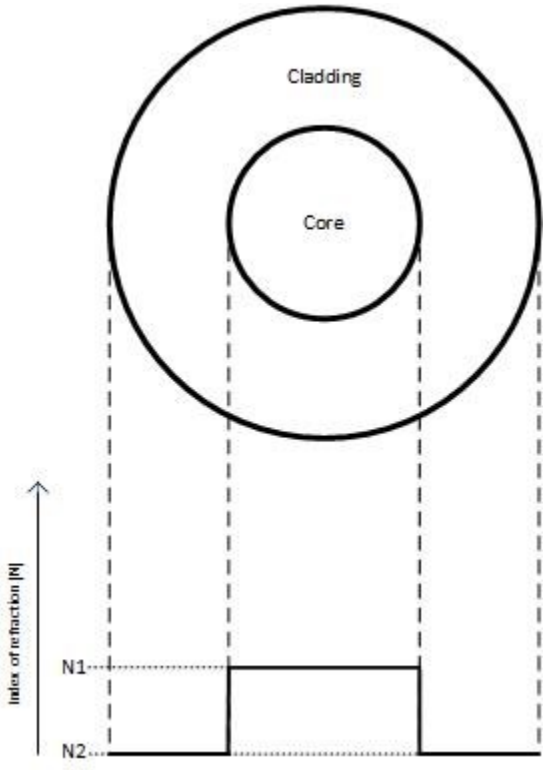

Figure 2-1 The cross section of typical single-mode telecommunication optical fiber with the refractive index profile.

In a fiber optic sensor, the heart of the senor is an optical fiber. An optical fiber in its simplest form is a cylindrical symmetric structure consisting of a central “core” surrounding by “cladding’. The refractive index profile of an optical material is depicted in Figure 2-1. The refractive index of a

core region is higher than the surrounding region, called cladding. The fiber core and cladding usually made from silica. The light trapped in the core of the fiber by total internal reflection at core-cladding boundaries. The light can travel in the fiber tens of miles with a little attenuation in the 1550 wavelength region[1].

Telecommunication via optical fiber waveguides has many roots and evolved during the time. The first introduced low loss fiber had a few dB Km^{-1} losses and the loss of present fiber is 0.2 dB Km^{-1}. In researches, several random materials added to the fiber in order to check the influence on the loss of the fiber optic. Germanium is one of the most used dopants within silica fiber. It replaces the silicon atom in the tetrahedral structure and bond with four oxygen atoms due to it belongs to Group IV A. Fused silica has a band-gap at around 9 eV. The band-gap of pure germania is at around 185 nm. These pure materials play a significant role in the attenuation profile of the waveguide and presence of the impurities causes absorption loss to be significant. The OH^- ion has infrared (IR) absorption at three wavelengths of 1.37, 0.95, and 0.725μm, the overtone is at a fundamental wavelength of 2.27 μm [8]. Defects inside the fiber lies within ultraviolet (UV) and visible wavelength band of 190-600 nm and increase the absorption.

Formation of fiber grating was first reported in 1978, but intensive research on this field was done after development on effective method of fabrication in 1989. Fiber grating have known to be useful in many field such as add/drop filters, amplifier gain flattening filters, dispersion compensator, fiber laser and many other application of optical communications. Some of the research led to commercialized product in this field[9].

Fiber Bragg grating has attracted considerable attention recently because of their numerous applications in fiber optic technology. The gratings generally are using as a narrowband reflection filter centered at the Bragg wavelength because of the stop band associated with a one-dimensional periodic medium [27]. During the past few years, the usefulness of fiber Bragg grating (FBG) for sensing and optical communication systems and devices has become fully apparent. Fiber Bragg

gratings FBG have been used in several devices and systems such as the wavelength division multiplexer WDM, dense wavelength division multiplexer DWDM, optical filter, laser, and optical add/drop multiplexer OADM. Fiber Bragg gratings can use in field of sensing as a strain and temperature sensors.

Since the early 1990s, fiber Bragg grating (FBG) sensors have developed due to their many desirable advantages such as the small size, absolute measurement capability, immunity to electromagnetic interference, wavelength multiplexing, and distributed sensing possibilities [10]. Thus far, the FBG sensors' capability to measure physical quantities such as the temperature, strain, pressure, etc., has been studied extensively. However, the use of FBG sensors for detection of environmental refractive index change has not been fully explored. Refractive index sensing is important for biological and chemical applications since a number of substances is detectable through measurements of the refractive index.

2.1 Properties of Fiber Bragg gratings

Bragg grating are refractive index structure manufactured by exposing the core of an optical fiber to intense ultraviolet radiation. The clear definition for photosensitivity is, its ability to change the refractive index with radiation within the fiber core. In The following a brief introduction to fiber Bragg gratings and its photosensitivity is provided.

Figure 2-2 shows the simplest form of the fiber Bragg grating consist of modulation of index of refraction in the core of the single-mode fiber. As it is clearly depicted in the figure, the phase fronts are perpendicular to the fiber longitudinal axis and the grating planes have constant period, which are the characteristics of uniform Bragg grating. The light couple along the fiber core and will experience the scattering by each grating plane[11]. If the Bragg condition is satisfied, the reflected light from each grating plane will add constructively to form back-reflected peak with

center wavelength defined by the grating parameters. In case of the Bragg condition is not satisfied, the reflected light from each planes become out of phase, interfere destructively, and cancel each other.

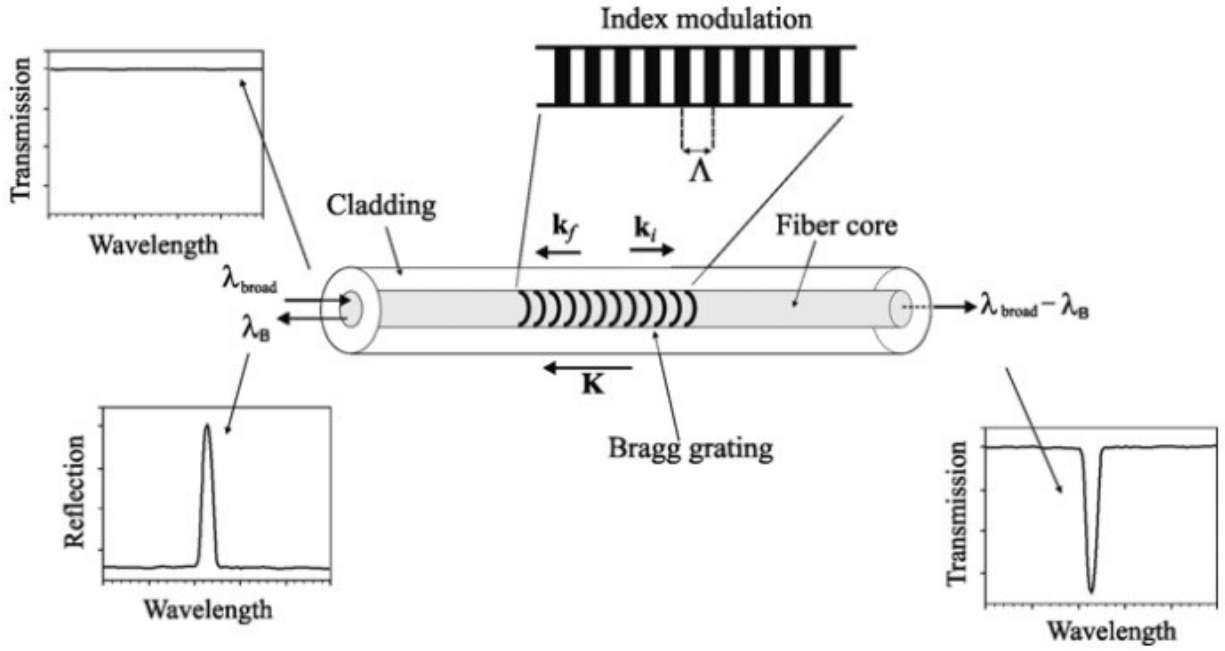

Figure 2-2 Uniform Bragg grating [12].

The Bragg grating condition, which discussed in previous paragraph, can be simply define as satisfaction of energy and momentum conservation. The energy conservation ($\hbar\omega_f = \hbar\omega_i$) is that similarity in the frequency of the incident light and the reflected light. The momentum conservation can be define as the incident wave vector,κ_i, plus the grating wave vector, κ, will be equal to the scattered radiation wave vector, κ_f. The related equation can be simply write as

$$\kappa_i + \kappa = \kappa_f \qquad 2\text{-}1$$

Where the direction of the grating wave vector, κ, is normal to the grating planes and its magnitude is $\frac{2\pi}{\Lambda}$ which is proportional to the spacing of grating,Λ, which is depicted in Figure 2-2. The wave

vector of the diffracted radiation is equal in magnitude but it has opposite direction from the incident wave vector. The momentum conservation condition can be write as

$$2\left(\frac{2\pi n}{\lambda_B}\right) = \frac{2\pi}{\Lambda} \qquad 2\text{-}2$$

By simplifying the equation, the Bragg condition can be extracted as

$$\lambda_B = 2n\Lambda \qquad 2\text{-}3$$

Where $\lambda_B$is the Bragg grating wavelength, n is the effective refractive index of the fiber core at the free-space-center wavelength. In the following, some properties of uniform Bragg grating will discuss.

2.1.1 Uniform Bragg Grating Reflectivity

The simplest fiber Bragg gratings structure in optical fiber is an axial and periodic change of the refractive index in the core, which is called uniform Bragg grating. Figure 2-3 schematically shows the refractive index modulation and effective refractive index of the grating structure. The refractive index modulation is given by:

$$n(z) = n_{avg} + \Delta n \ cos(\frac{2\pi z}{\wedge}) \qquad 2\text{-}4$$

Where n_{avg} is the average refractive index of the structure, Δn is referred to as the modulation amplitude (typically$10^{-5} - 10^{-2}$), z is the axial position and $\wedge$ is considered as geometrical grating period.

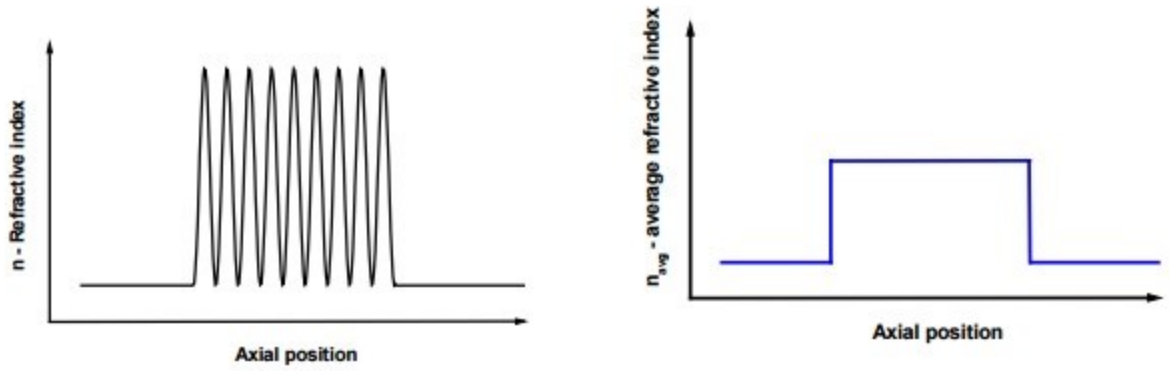

Figure 2-3 Refractive index modulation and effective refractive index of the grating structure [13].

As mentioned in previous section, the reflected wavelength of this structure follows the equation of

$$\boldsymbol{\lambda}_B = 2\, n_{avg} \wedge \qquad 2\text{-}5$$

Where n_{avg} is the average, or effective refractive index of the core along the grating. The spectral reflectivity of the grating is achieved with using the coupled-mode theory, is given by[14]

$$R(l,\lambda) = \frac{\Omega^2\, sinh^2(sl)}{\Delta\beta^2\, sinh^2(sl) + s^2\, cosh^2(sl)} \quad for\ \Omega^2 > \Delta\beta^2 \qquad 2\text{-}6$$

$$R(l,\lambda) = \frac{\Omega^2\, sinh^2(Ql)}{\Delta\beta^2 - \Omega^2\, cosh^2(Ql)} \qquad for\ \Omega^2 > \Delta\beta^2 \qquad 2\text{-}7$$

Where $R(l,\lambda)$ is the reflectivity, which is function of the length of the grating (l) and the wavelength (λ). Ω is the coupling coefficient, $\Delta\beta = \beta - \frac{\pi}{\Lambda}$ is detuning wave vector, k is propagation constant and is equal to $\beta = \frac{2\pi n_\circ}{\lambda}$, and $s = \sqrt{\Omega^2 - \Delta\beta^2}$. $Q = iS$ For the single mode sinusoidal modulated grating. For the sinusoidal variation of index of perturbation, the coupling constant can describe as

$$\Omega = \frac{\pi\, \Delta n\, \eta(V)}{\lambda} \qquad 2\text{-}8$$

In this equation η is the fraction of the fiber mode power contained by the fiber core and its value is $\eta(V) = 1 - V^2$. Where V is the normalized frequency of the fiber and it can calculate using $V = (\frac{2\pi a}{\lambda})\sqrt{n_{co}^2 - n_{cl}^2}$, where the term a is the radius of the core, and n_{co} and n_{cl} are the refractive indices of the core and cladding, respectively.

$\Delta\beta = 0$ At the Bragg grating center wavelength and there is no wave-vector detuning, hence, the simplified form of equation 2-6 become

$$R(L, \lambda) = tanh^2(\frac{\pi \Delta n L}{\lambda}\eta) \qquad 2\text{-}9$$

Where L is the length of the grating, λ is he reflected wavelength, and η is the overlap between the fundamental mode and core [14]. Typical values for the η is equal to 0.8 and 0.9.

Figure 2-4 is the simulation of the reflection spectrum for a 10 mm long grating with a uniform index modulation of the$\Delta n = 1 * 10^{-4}$. It is possible to achieve desirable properties by controlling the refractive index modulation and average refractive index along the grating.

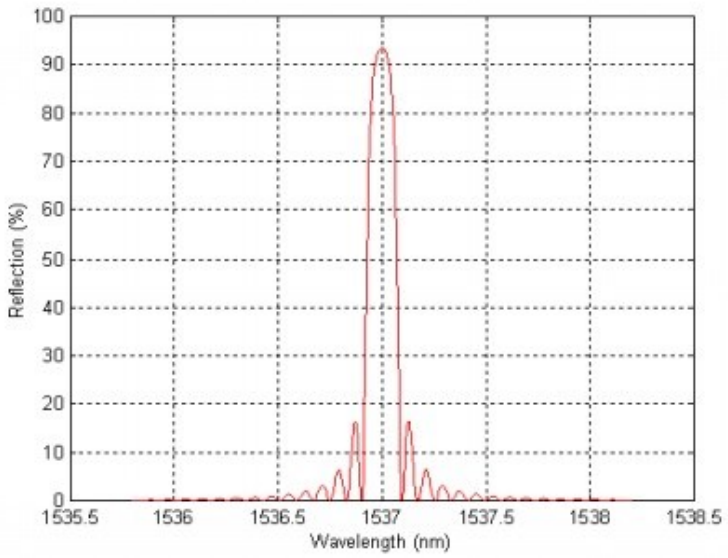

Figure 2-4 Simulation of the reflection spectra of a 10 mm long uniform grating as a function of wavelength ($\Delta \boldsymbol{n} = \mathbf{1} * \mathbf{10^{-4}}$) [13].

The spectral full-width half-maximum of the grating is given by [15]:

$$\Delta\lambda = \lambda_B \sqrt[s]{(\frac{\Delta n}{2n_0})^2 + (\frac{1}{N})^2} \qquad 2\text{-}10$$

Where the N is the number of fringes (typically N∼20000 for the 10 mm long rating) and the pre-factor s is equal to 0.5 for the weak grating and is equal to 1 for strong grating

2.2 Classification of fiber Bragg grating

There are five different types of grating depending on the coupling function. Figure 2-5 schematically depicted different types of fiber grating. As completely described in previous section, under satisfactory of Bragg grating conditions, a fiber Bragg grating couples the forward propagating core mode to the backward propagating core mode. In part (b), long period fiber grating (LPG) is depicted, which couple the forward propagating core mode to one or few of the forward propagating cladding mode. Part (c) schematically depicted chirped fiber grating which has a wider reflection spectrum. Each of the wavelength component experience different position, hence, result in a delay time difference for different reflected wavelengths. A tilted fiber grating, which depicted schematically in Figure 2-5 (d), couple the forward propagating core mode to the backward propagating for both of core and cladding mode. The last fiber grating which is shown in Figure 2-5 described the type of the fiber grating called sampled fiber grating that can reflect several wavelength components with equal wavelength spacing. All of described fiber grating are utilized in various types of fiber grating sensors and wavelength change interrogators. Among all of them, fiber Bragg grating (FBG) have been widely used as a sensor head and shows most satisfying results[9].

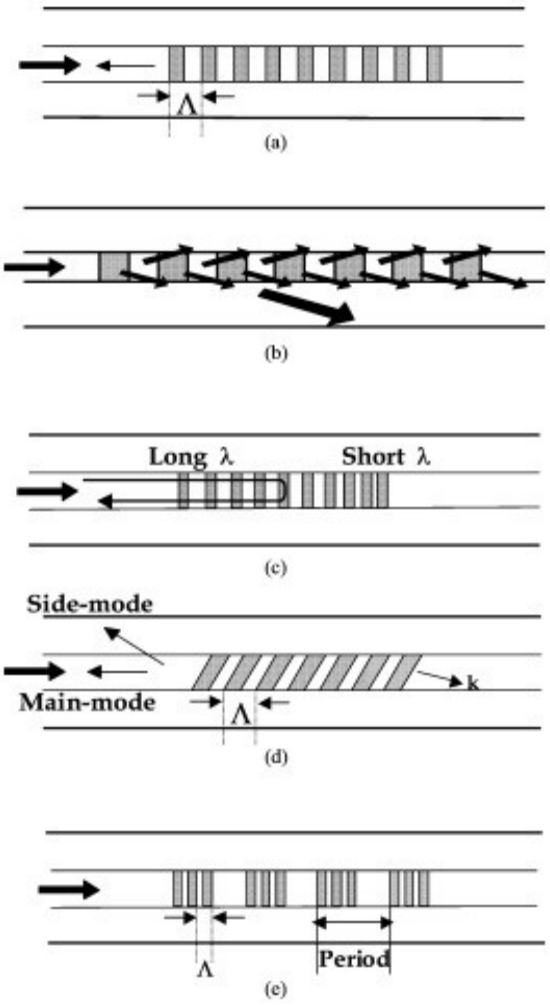

Figure 2-5 Types of fiber gratings. (a) Fiber Bragg grating, (b) long-period fiber grating, chirped fiber grating, (d) tilted fiber grating, (e) sampled fiber grating [9].

2.3 Methods for fiber Bragg grating fabrication

Fiber Bragg grating is a periodic perturbation of the refractive index along the fiber length which is formed by exposure of the core to an intense optical interference pattern [16]. In very first experiments, intense Argon-ion laser radiation was launched into a germania-doped fiber. The result was after several minutes the reflected light intensity increased until the almost all the light was reflected from the fiber. This grating known as a "Hill grating" which operates at wavelength

of near writing wavelength[7]. Using this achievement, many researches done on the different properties of germania-doped silica fiber and different fabrication methods.

To meet the requirements of communication and sensing application, many researches on the subject of fabrication techniques have been done for many years. A number of schemes are introduced to achieve the ideal fiber Bragg grating with desired features such as flexibility, economical mass production, good physical and optical qualities, and good repeatability. Many of methods has led to successful commercialization of the fiber Bragg grating. Primarily, methods of fabrication divided into two sub group including the two-beam interferometer method and the phase-mask method [7]. In this study, we review the phase-mask fabrication technique.

2.3.1 Phase-mask technique

Phase-mask is fabrication method that is reported by Hill et al and Anderson et al in 1993 as an improved method for the fiber Bragg grating fabrication technique. The phase-mask itself is a diffractive element that is used for creating the interference pattern; such as Bragg grating pitch, with the spatially phase modulated and diffracted by the phase-mask light beam. Figure 2-6 is schematically depicted the phase-mask fabrication method of fiber Bragg grating. The interference pattern which clearly drown in Figure 2-7 is used for photoimprinting a refractive index modulation in the photosensitive fiber right behind the phase-mask in vicinity and parallel.

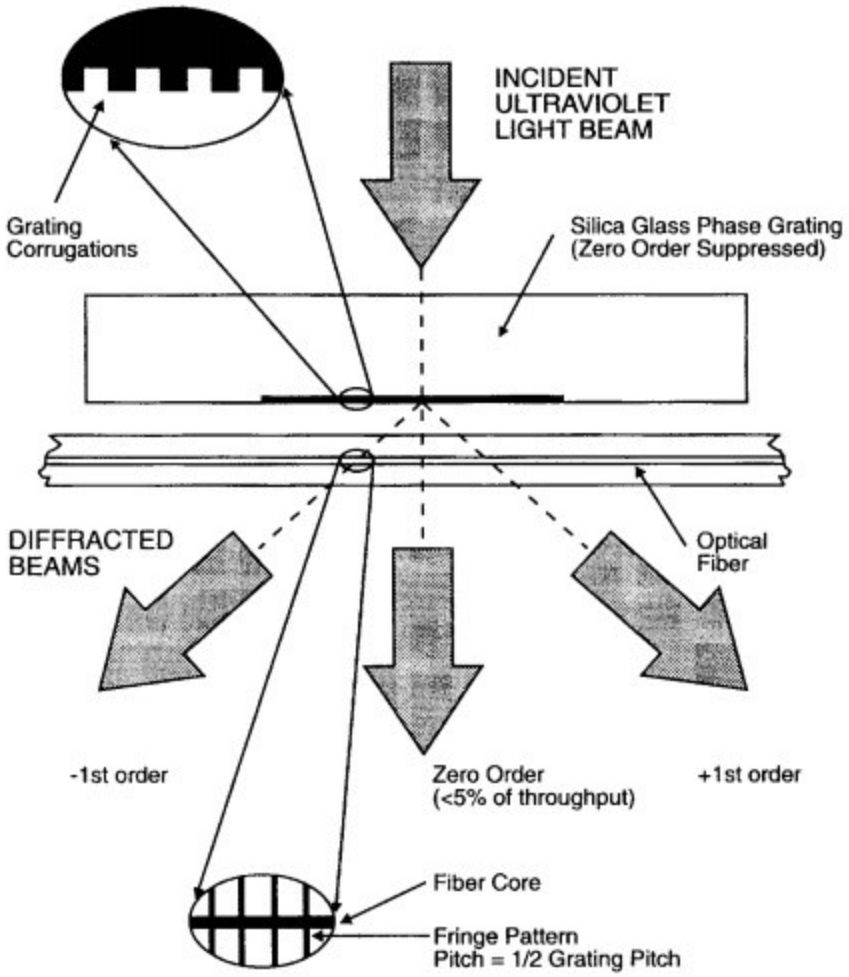

Figure 2-6 Schematic of the phase-mask fabrication method [17].

Phase-mask introduces many advantages over the two-beam interferometer technique. The first advantage of using phase-mask is the Bragg wavelength can be determined by the pitch of the phase-mask and it is completely independent of the UV light beam. Second, the phase-mask offers a high probability of mass production with good repeatability at low cost due to the phase-mask method is used under a computer controlled photolithographic imprinting process through an original phase-mask. Furthermore, it is easy to use in practice due to it is single-beam writing process, it improves the mechanical stability of the FBG writing apparatus significantly. In addition, the UV laser which is used for two-beam interferometer is highly coherent and it is

expensive, but phase-mask technique needs less coherent UV laser is reduced and hence low spatial and temporal coherent can be used to write grating.

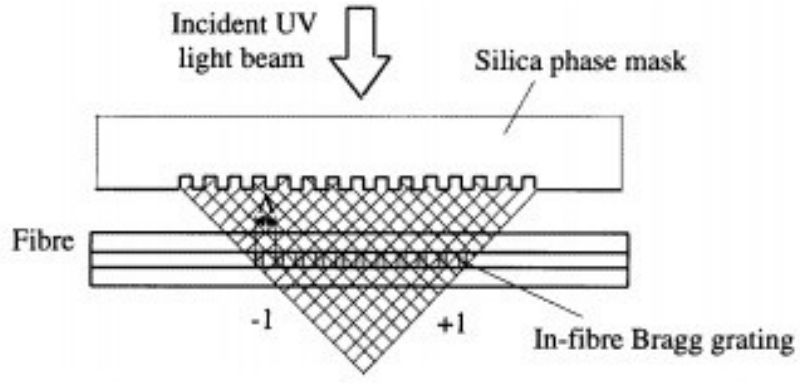

Figure 2-7 Interference pattern of the phase-mask writing method [18].

2.4 Photosensitivity of Fibers

2.4.1 History of photosensitivity

Photosensitivity in fibers first has been seen by Hill and co-workers in communication research center in germanium-doped silica optical fiber waveguide [19]. In optical fiber waveguide there is photosensitivity that is inseparable characteristic for photoinducing permanent refractive index changes inside the core of the optical fiber. photosensitivity proved to exist in several types of planar glass structure such as silica-on-silicon, and silica-on-silica planar waveguide devices in addition to the fiber structure [17].

In this part of the study, definition of three terms of photorefractivity, photosensitivity and photochromic effect make it easy to distinguish between these three concepts. Photorefractivity can be defines as the sensitivity of a material property to light. This effect is a nonlinear optical effect exist in certain crystals and other materials that respond to light by altering their refractive index [20]. It is well known that during UV-irradiation of germanosilicate optical fibers and glasses, several physical processes proceed simultaneously and lead to a refractive index

change. These processes are usually referred to as different photosensitivity types [21]. The last term, photochromic, refers to change in color of the glass during the exposure to ultraviolet radiation and heat. The process is reversible due to during the procedure the glass does not apply to change the opacity by heat. The combination of these properties is feasible inside the glasses, it is the novel phenomenon, and it is under studies.

For almost a decade after the first discovery in Canada, research on photosensitivity of fibers was followed by the specially designed Bell Northern research fiber. The research group, Lam and Garside in 1981 [14], find out that the writing power has the direct impact on the amount of the photoinduced refractive index change. The refractive index change with respect to the square of the writing power at the argon ion wavelength (488 nm). In this study, a two-photon process was introduced as mechanism that is responsible for changing the refractive index. Due to there was no international interest in fiber photosensitivity at the time, the effect only being studied for a prepared fiber. Almost a decade later, Stone [22] was examining the photosensitivity of fiber in so many different fibers. He used the heavily doped fiber with germanium.

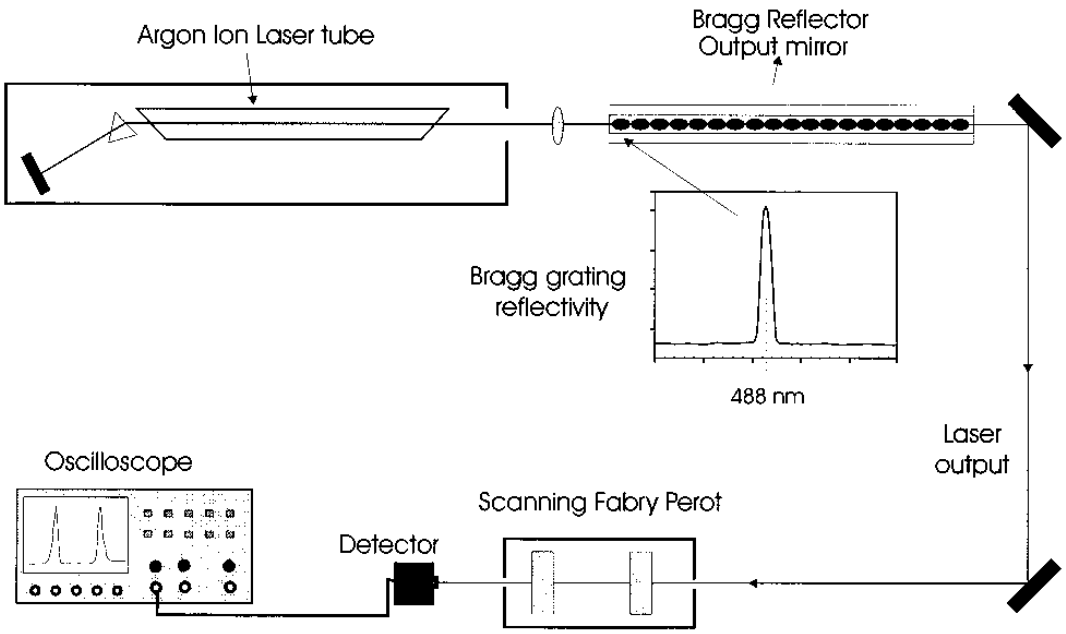

Figure 2-8 CW distributed feedback argon ion laser. The fiber reflection filter (~1m long) takes the place of output reflector and gives rise to narrow band oscillation [23].

Hill and co-workers [23] were first discovered the Bragg grating. They used the experiment to study the losses in a specially designed germanosilicated fiber optic. They have placed the germanium heavily doped fiber Bragg grating in the output reflector of an argon ion laser. An argon-ion laser was focused to core of the fiber using microscope (a*32) objective lens. The output intensity of light from fiber end is gradually decreased as the time passed. Running other experiments, they found out that the reflected intensity has increased[24]. Figure 2-8 schematically shows the configuration which they used to study the phenomenon. This was the first reported distributed feedback oscillation of a gas laser which is worked in the visible region of the spectrum. The output reflector was detached from the laser head and a microscope (a*32) objective lens was used to couple the beam into the core optical fiber core which have a reflection filter.

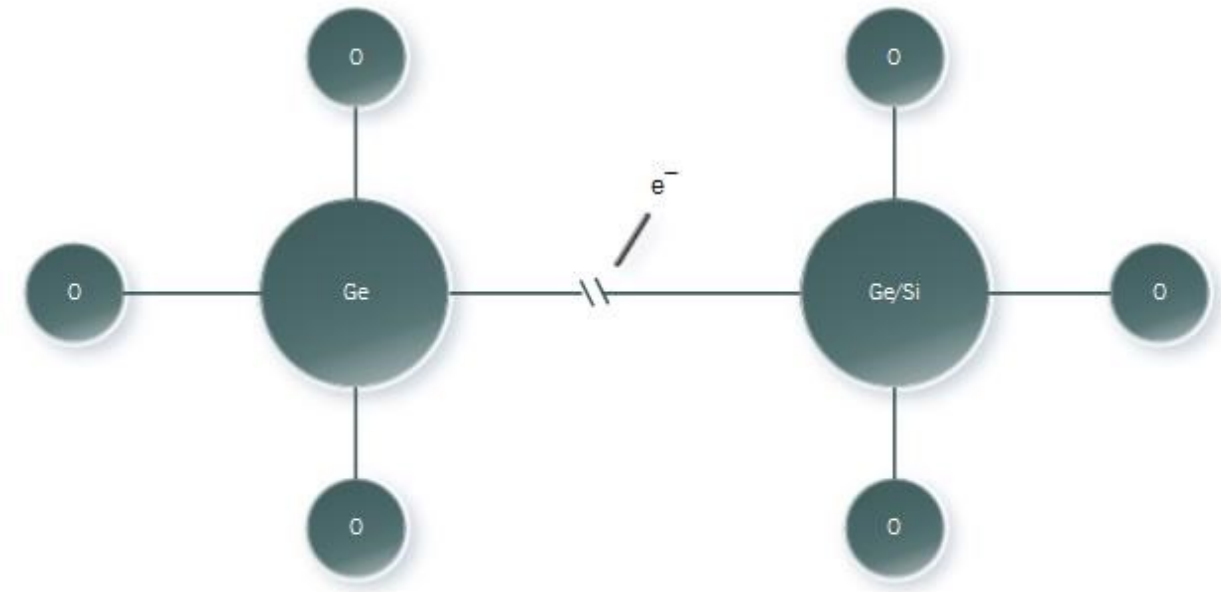

Figure 2-9 oxygen deficient germania defects thought to be responsible for the photosensitive effect in germania-doped silica. An electron is released on breaking of the bond [11].

The strong index of refraction has been achieved by Meltz et al. in 1989 with simply exposing the germanium-doped fiber to the ultraviolet (UV) light [25]. The fiber was exposed to UV light close to the germania-related defect peak absorption at a wavelength range from 240 nm and it is related to the defect called germanium oxygen deficient center (GODC). Figure 2-9 schematically depicts the oxygen-deficient germania defect, which is one of the mechanism responsible for the photosensitivity in germania-doped silica. The GeO defect has peak wavelength absorption at ~240 nm. Figure 2-10 is depicted absorption at 240 nm is bleached when exposed to UV radiation.

In 1989, Hand and Russel, with Kramer-Kroning relationship developed a model to show the change in the refractive index related to the absorption. The model that proposed shows the breaking of the GeO defects resulting in a GeE' center with electron free to move. This free electron can move within the glass until is trapped by bond either at the same site or another location within the molecule lattice. There is a vast number of researches that is done on fibers, which are doped with materials other than germanium, and they showed the photosensitivity.

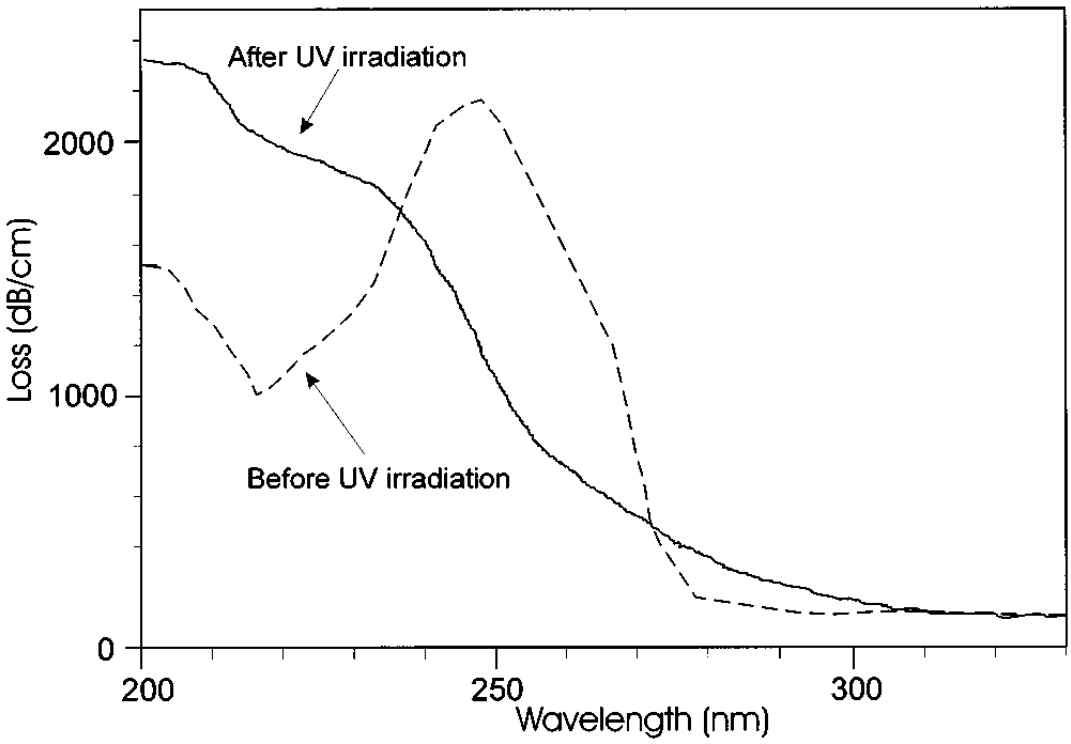

Figure 2-10 Transmission loss spectrum of a 15 µm thick which is shown before and after UV radiation at 244 nm[26].

2.4.2 Defects in germanosilicate optical fiber

The fact that change in the index of refraction in germanosilicate optical fiber is triggered by a single photon process at energies well below the band gap in 146 nm, implies that the point defects in the ideal glass tetrahedral network are responsible for this process. At first, the defects draw the attentions because of their transmission loss due to undesirable absorption band associated with them. However, by development of fiber Bragg grating, the role of the defects in optical fiber has changed dramatically.

Major studies and important photosensitive fibers are based on germanosilicate fiber. Germanium (Ge) has two moderately stable oxidization states, +2 and +4, unlike Si. Therefore GeO and GeO_2 can be found inside the silica glass. It is well known the GeO is more stable than GeO_2 at high temperature. The chemical reaction which is happen inside the modified chemical vapor deposition (MCVD), process is based on hot gasses reaction to creating a soot deposit on the inside of a silica

support tube or on the outside in the outside vapor phase deposition (OVD). The result of this process is oxygen deficient matrix. It is feasible that the GeO molecules exist inside the germanosilicate fiber in discrete, but it is very likely to manifest itself in the form of Ge-Si wrong bonds, suspected defect precursors[27].

The silica fiber which is doped with germanium, forms suboxides as GeO_{χ} (χ= 1 or 2), creating a range of defects in the tetrahedral matrix. Although germania-doped silica fiber has rich environment of imperfection, it has extremely good properties, such as low loss and high optical damage threshold [7].

Friable et al., first pointed out the well-known defect formed in the germania-doped silica core which is named paramagnetic Ge(n) defects. In Ge(n) the term n refers to the number of nearest neighbor Ge/Si atoms surrounding a germanium ion with an associated unsatisfied single electron. A variety of mechanism known to be responsible for the change in the index of refraction. It is generally accepted in the literature that the formation of particular point defects associated with germanium play a significant role in the photosensitive response. Figure 2-11 schematically depicted the defects responsible for change in the index of refraction. By increasing the germanium content inside the fiber core the number of germanium oxygen deficient center (GODC) is increasing. The Ge(1) and Ge(2) are trapped electron center (in the structure there is free electron). The GeE', that is known previously as the Ge(0) and the Ge(3) centers, is a hole trapped next to the germanium at an oxygen vacancy and it is independent of the number of neighboring Ge site which is common in oxygen-deficient germania. In tetrahedral structure, one oxygen atom is missing so the germania has an extra electron with dangling bond. The two defects that known to play a significant role are the Ge^{2+} defect with and absorption band at 241 nm and neutral oxygen vacancy (NOV) with an absorption band lies at 245 nm. The NOV is the wrong bond between Ge-

Ge or Ge-Si rather than Si-O-Ge or Si-O-Si. Figure 2-12 schematically shows the extra electron distorts the germania molecule.

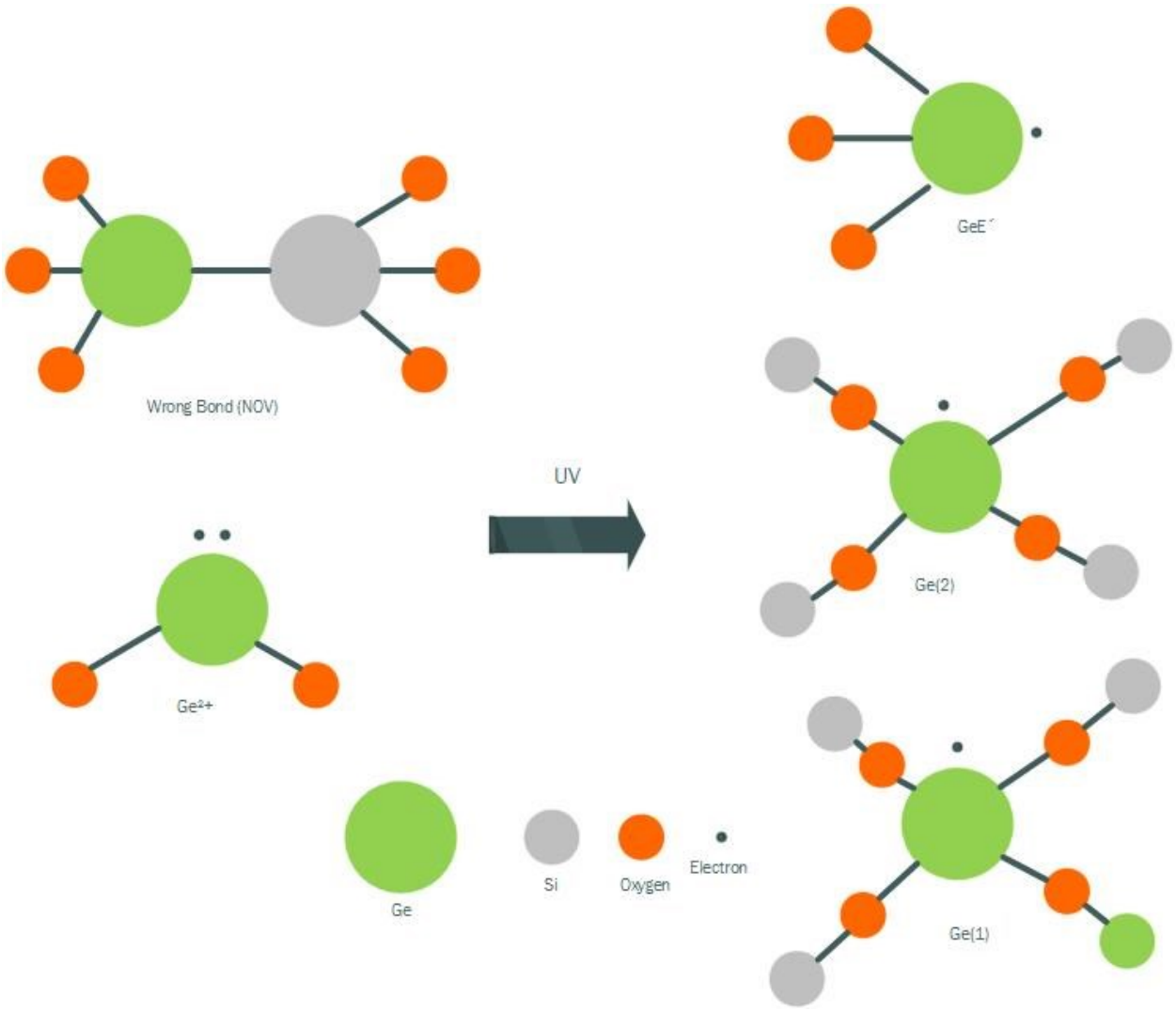

Figure 2-11 Common point defects of germanosilicate thought to be responsible for photosensitivity. GODCs (left) which are believed to absorb around 244 nm and produce the GeE' defect and liberate electrons which are captured to form Ge(1) and Ge(2) sites (right)[7].

As shown in Figure 2-12 (a), the GeO defect has a germanium atom coordinated with another Ge or Si atom. It has been observed in many germanium-doped photosensitive optical fiber that this bond has peak absorption band is at 240 nm [28]. By UV exposure, the bonds are broken and create

the GeE'. The electron from the GeE' center is free to move within the glass matrix via hopping or tunneling or by two-photon excitation into the conduction band [7]. The free electron can be trapped at original site or at wrong site that is created by defect. It is thought that removing this electron can change the shape of the molecule and can change the density of molecule as well as absorption, as shown in Figure 2-12. It is observed that the Ge(1) center is the same as germanium defect in α-quartz, named as Ge(I) and Ge(II) but it is less well defined. Although Phosphorous doped silica glass can form defects, which is similar to germanium defects, its photosensitivity is limited at 240 nm; so the radiation should be shorter than 240 nm such as 193 nm. The nonbridging oxygen hole center (NBOHC) defects have absorption at 260 and 630 nm, also the peroxy radical (P-OHC) has an absorption at 260 nm as shown in Figure 2-11.

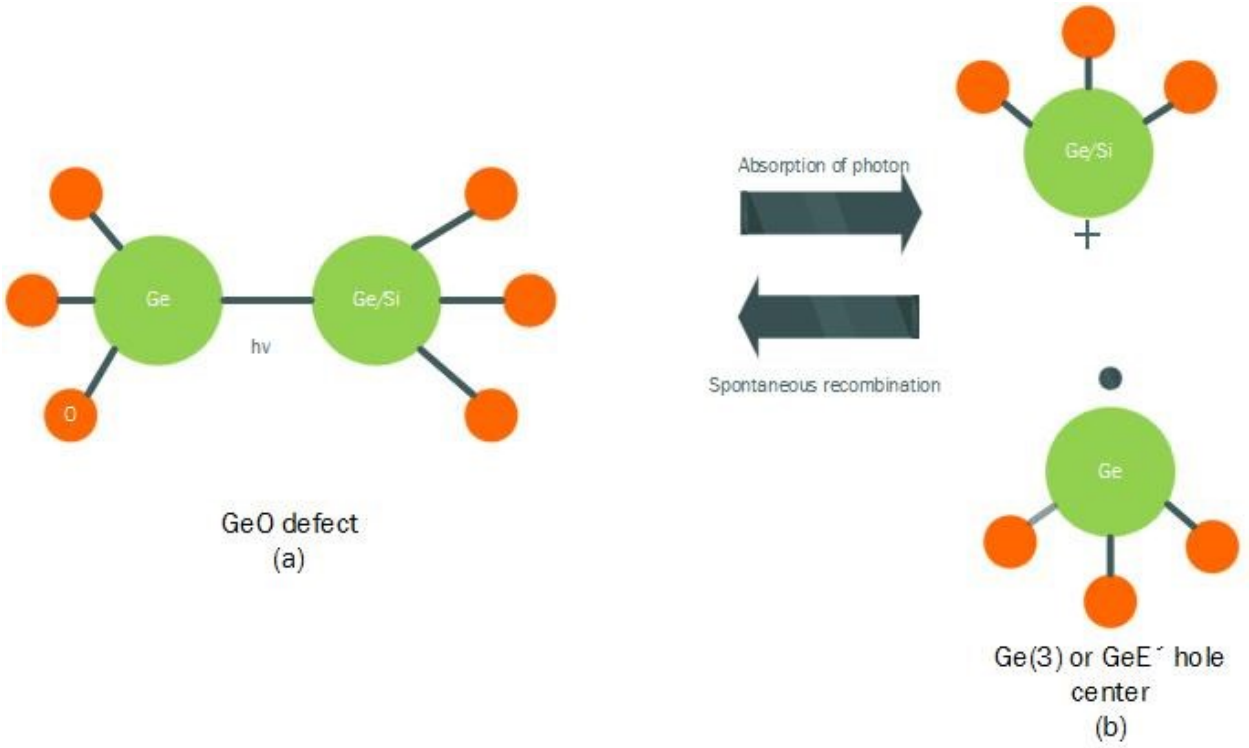

Figure 2-12 The germania-doped silica fiber GeO defects, in which the germanium atom bonds with either silicon or germanium. If the defect absorbs a photon it can form a GeE' defect. The GeE' center is Ge(0) or Ge(3). The GeE' has an extra electron (

associated with the Ge atom) which is free to move in glass matrix until it traps at original defect site, at hole site of another GeE', or at any of the Ge(n) defects [7].

2.5 Photosensitization Techniques of Fiber Bragg Grating

The standard telecommunication fiber is the most preferable one in order to write the strong grating in this type of the fiber. The writing the grating in this type of fiber is well established but it is not suitable for number of the applications. A compatibility of the standard fiber is desirable, but for designing different kind of devices, various type of fibers are needed. This can cause the use of different kind of technique for fabrication and sensitization. Some commonly used species of optical fiber have been reviewed by their behavior and properties and their type of application. The tie and intensity of the exposure of UV, which is used for writing the grating, for example, influence on the reliability and transmission properties of fiber. This results in damage (Type II A gratings) or at low radiation formation of type I, and type II A gratings, each of them has distinguished characteristic.

It has been proved that photosensitivity of optical fibers is correlated with the concentration of GeO defects in the core. As a function of germanium concentration increase, the number of defects increases. Figure 2-13 shows the absorption at 242 nm in sample with the germanium concentration [29]. The graph indicates that the slope is ~28 dB/(mm-mol%) of Ge before the utilized sample is collapse. After collapse the absorption changes to ~36 dB/(mm-mol%), which indicated that the number of defects increases.

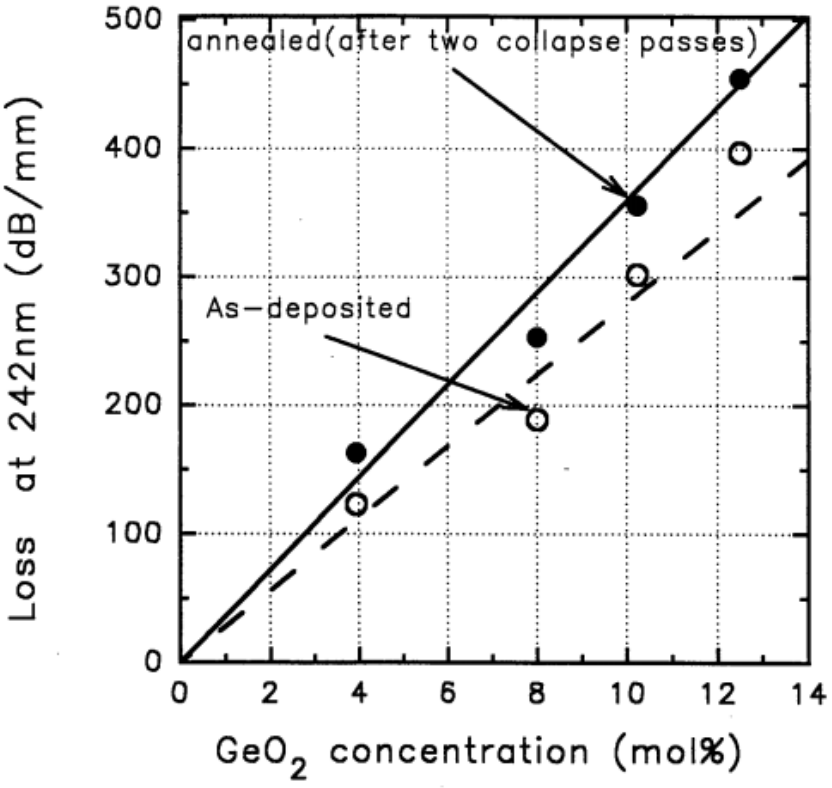

Figure 2-13 Absorption at 242 nm in preform samples before and after collapse as a function of Ge concentration [29].

Increase in concentration of defects, attribute to increase the photosensitivity of fiber. This can be done by collapsing the fiber in a reducing atmosphere, for example, by replacing oxygen with nitrogen or helium, or with hydrogen [29].

UV-induced fiber Bragg gratings have been shown to have great importance in recent years, and they have wide range of application in fiber optic sensing and application in fiber optic sensing and telecommunication. The effect of boron in Germania-doped silica glass known for long time. Doping the germanosilicate fiber with boron reduces the refractive index. Many changes have been done depend on the thermal history and processing of the glass. As an example of this changes, it

is generally used in the cladding of optical fibers, due to the core region must have the higher refractive index [30].

Some techniques are developed in order to increase the amount of defects inside the fiber core and thus increase the photosensitivity of fiber Bragg grating. Germanium doping of silica fiber is one of the most developed technique in order to increase the photosensitivity. The other method is germanium-boron co-doping of silica fiber. In addition, tin-germanium co-doping is the developed technique to increase the number of defects. Cold, high-pressure hydrogenation is the subject of vast number of researches due to that the presence of molecular hydrogen increases the absorption loss in the optical fiber. The result is because the hydrogen reacts with the oxygen to form hydroxyl ion. The flame brushing is a technique to brush the region of the optical waveguide with a flame fueled with hydrogen (hydrogen-rich flame) and the small amount of oxygen repeatedly for photosensitization.

3 System design

The advantages of optical fiber sensing are well known and this filed been widely established in the research literature. However, optical fiber sensors experience the few real commercial successes, and the technology remains in the laboratory experiments. Many fiber optic sensors were developed to use in a place of conventional electro-mechanical sensor system, which are well established, reliable and relatively are low priced compare to the existing sensors. The fiber sensors introduce important advantages such as electrically passive operation, electromagnetic interference (EMI) immunity, multiplexing capabilities, high sensitivity but its development is very slow. In compare with other kind of sensors, fiber sensors offer new capabilities, such as distributed sensing. Fiber Bragg gratings (FBGs) and other gratings-based devices are the proof of the type of sensors which have the mentioned capabilities[31].

Gratings are simple, intrinsic sensing elements which are photo-inscribed into the silica fiber [32] and also introduce all the advantages of fiber sensor. One of the distinctive capabilities of the gratings is the devices have an inherent self-referencing. In addition, many sensors can multiplexed along a single fiber easily. Grating-based sensors are appropriate for wide range of applications. One of the most primary interests is creating “smart structure” with distributed embedded sensing in materials. Fibers with sensor arrays can used for measuring parameters such as temperature, strain, load, and vibration and the health of the structure and track of the parameters can be done on a real-time basis. Gratings also introduce as the optical sensing element in some other range of fiber sensor application such as grating based chemical sensors, accelerometers, and pressure sensors.

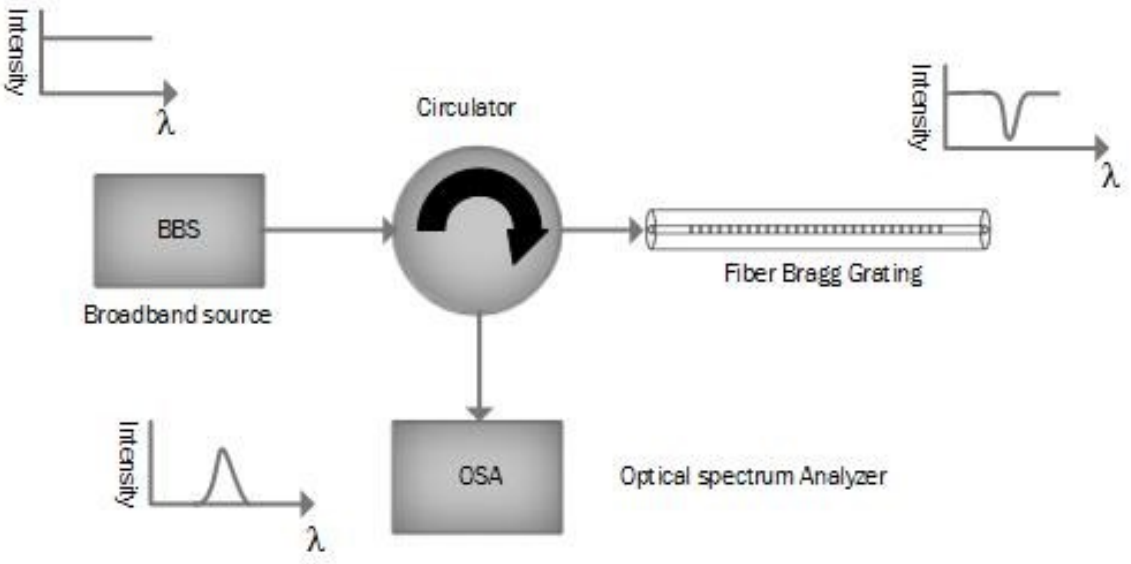

Figure 3-1 schematic of the interrogation system using OSA.

The principle of the FBG temperature sensor is based on the measurement of shift in the Bragg wavelength corresponding to variation in temperature [33]. In general, the shift in Bragg grating wavelength is monitored by using an optical spectrum analyzer (OSA). Figure 3-1 is schematically shows the sensor configuration. For many applications including our application, OSA has its own limitation. The limitation of OSA can be pointed as

- There is a limitation regarding the resolution of OSA.
- When we have high resolution respond from the OSA, the delay time respond will increase.
- The OSA is not an apt sensor interrogation system in some applications, due to its weight and size.
- The OSA is an expensive device.

Many techniques have developed in order to overcome the limitation of the OSA. Among all the introduced methods, the ones that are based on intensity modulation draws more attentions. In this method, photodetector is used instead of OSA. The simple system is converting the wavelength information into its equivalent intensity modulated signal, which can be measured by a photodiode.

The first reported intensity modulation system was reported in 1997 for measuring the strain[34]. They used the long period grating in their experimental setup. The light from erbium fluorescence source couples along the fiber Bragg grating, part of the light that meets the Bragg condition will reflects back and passes through the LPG. The long period grating having spectral loss at selected wavelength and act as a linear response edge filter to convert wavelength shift to intensity changes. The intensity of the transmitted light is altered. It can decrease, or increase (depending on which side of the LPG, is used in filtering) with the strain/temperature-induced wavelength shift of the FBG.

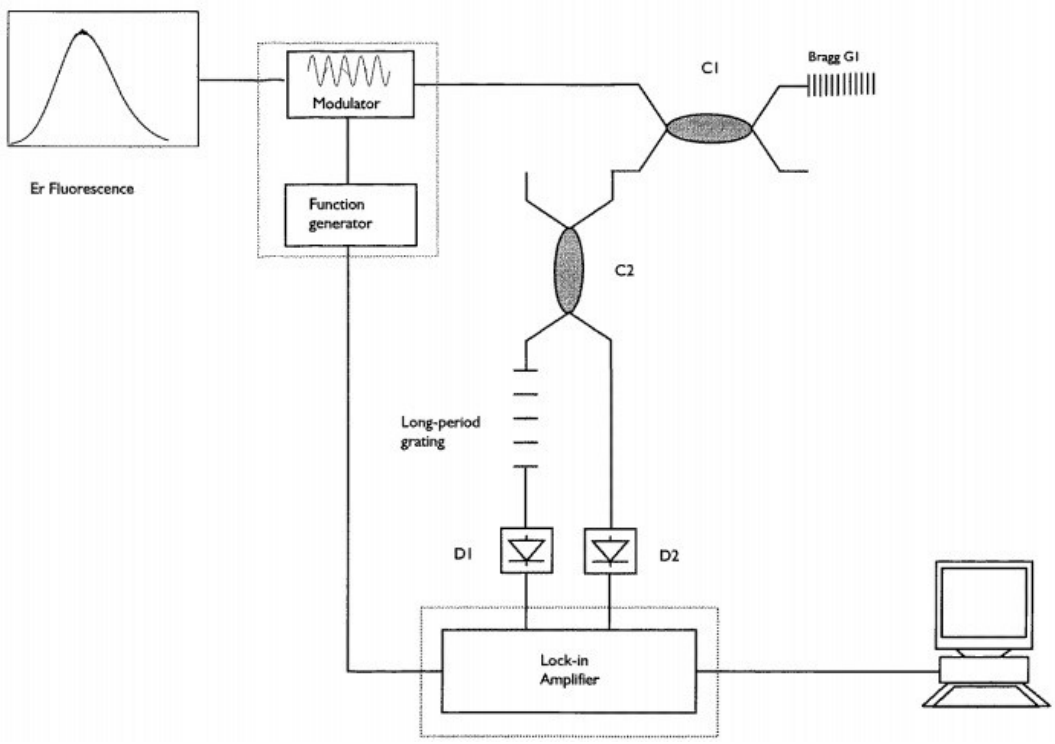

Figure 3-2 Experimental set-up for fiber grating sensor intensity modulation interrogation system. The dotted boxes outline the modulation system employed in the resolution improvement experiment [34].

Figure 3-3 is the schematic of one of the recently amplitude modulation method. In this method, the broadband light source (BBS) passes along the long period grating (LPG) and in its way, reaches the FBG. After the light passes through the LPG, the transmitted light experience the spectral loss and its amplitude decrease or increase (depends on the type of the LPG) linearly. Part

of the light, which meets the Bragg condition, will reflect back through the circulator and the rest of the spectrum passes the FBG. The Bragg spectrum then reaches the photodiode, then it is possible to measure the intensity of the reflected back light [35].

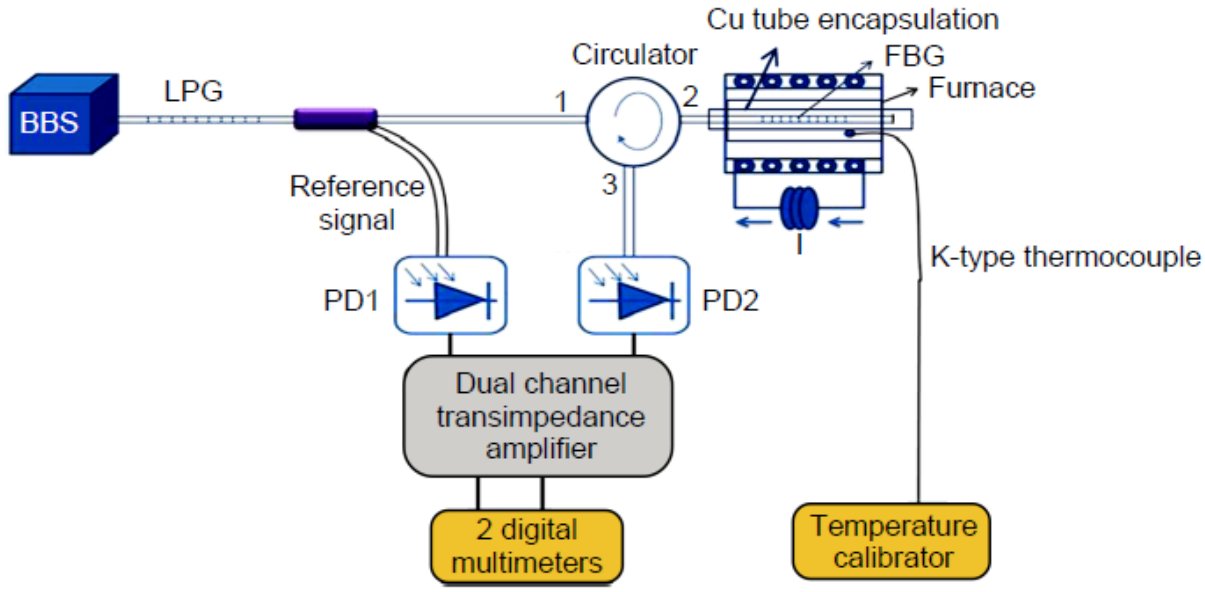

Figure 3-3 schematic of an experimental setup without using OSA [33].

3.1 Designed temperature sensor

In the like manner, we come up with the new idea to overcome the disadvantages of the frequency modulation interrogation system. We designed a high temperature sensor, our design is based on amplitude modulation with the same idea given in Figure 3-3. In our design, the ASE light source utilizes as a light source, due to its unique characteristics in its spectrum. The analyses of ASE light is given in chapter 4. Figure 3-4 shows the configuration of the designed high temperature sensor. In the design, an amplified spontaneous emission (ASE) light source, a splitter, two photodiodes, a 3-port optical circulator, and a fiber Bragg grating is used.

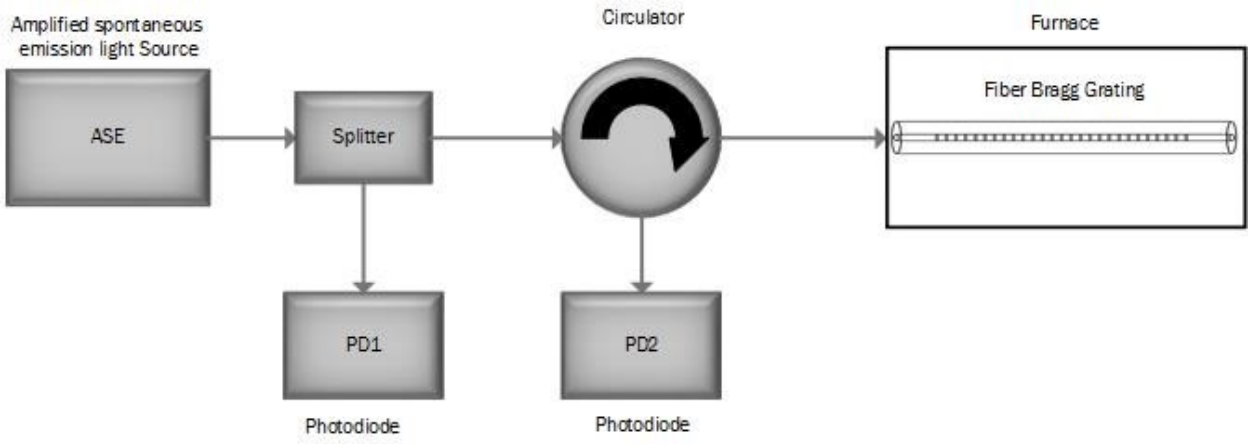

Figure 3-4 Configuration of the designed high temperature sensor based on fiber Bragg grating.

The hypothesis behind the designed sensor is, if we have the linear input light integrating along the fiber Bragg grating, then it is rational to say

$$\lambda_B \propto \frac{PD1}{PD2} \quad Equation\ 3\text{-}1$$

Where λ_B is the Bragg wavelength, PD1 is the power of the light source, and PD2 is the power of the Bragg backward spectrum. The equation says that there is the linear relation between the Bragg wavelength and the ratio of the$\frac{PD1}{PD2}$. The hypothesis is correct in the case when we use the linear spectrum light source. In our design, the input light source that choose for the temperature sensor is ASE light source. Figure 3-5 shows the spectrum of the ASE light source. It is possible to deduce from the figure that the ASE light source have some ranges that the spectrum is linear.

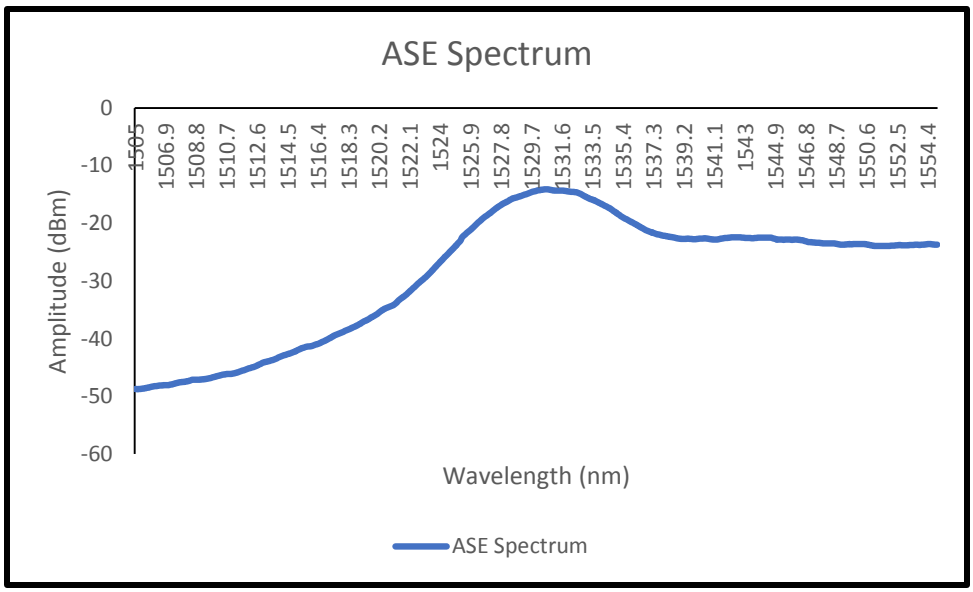

Figure 3-5 The ASE light source output spectrum.

The designed interrogation system provided in Figure 3-3, used the broadband source and long period grating (LPG) as a source to create the linear input light. The drawback of using LPG as a mean to create the linear input light is its high price. In this study, we design the high temperature sensor based on fiber Bragg grating with lower price. The ASE light source is used instead of broadband source and LPG. Figure 3-5 is clearing the idea of usage of ASE light source. Due to the possibility to find the linearity in its spectrum. As it is clear in the spectrum roughly in the range of 1523 nm to 1527 nm and in the range of 1533 nm to 1537 nm as well.

In Figure 3-6, using an ASE light source spectrum, we showed the idea beyond the designed temperature sensor. As depicted in the figure, we design the sensor head with Bragg wavelength in a range that the ASE light source spectrum is linear. In this figure (a) shows the initial Bragg reflected spectrum. By changing the ambient temperature of the FBG, the Bragg wavelength will experience a blue shift or red shift. In the figure, the reflected light of the FBG is shown as (b) for the case that ambient temperature is increased. As it is seen in the figure, there is a linear relation between the amplitude of the reflected light from the FBG and its shifted spectrum.

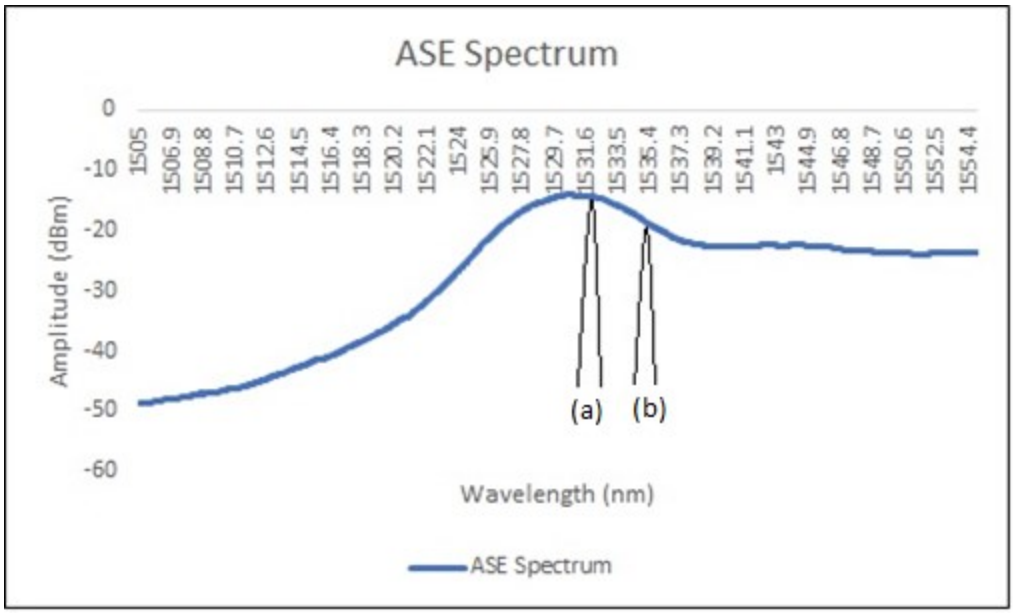

Figure 3-6 Working principle of the sensor followed by an interrogation system.

As it is shown in the figure, rather than interrogate the sensor with frequency modulation system, we focus on the amplitude modulation interrogation system because of its advantages. We tried to relate the amplitude of the backward reflected light of the FBG to temperature. In order to calibrate the sensor, we come up with measuring the change in the Bragg wavelength with respect to the temperature. We run up the temperature from -27 ºC to 400 ºC for two prepared sensor heads for several times. The result of this measurement are discussed in chapter 5.

Furthermore, after setup the system as shown in Figure 3-4, we can measure the ratio of $\frac{\mathrm{PD1}}{\mathrm{PD2}}$ with respect to temperature. By considering the relation between the Bragg wavelength and the temperature and the relation between $\frac{\mathrm{PD1}}{\mathrm{PD2}}$ and the temperature, it is possible to find the proportional constant of the equation 3-1.

4 Amplified Spontaneous Emission Light Source

Amplified spontaneous emission light source, also known as an ASE light source, is the low-coherence, wide-band light source. The ASE light source sometimes named as a Broadband light source or low-coherence light source. The output light has some distinguished features such as high-brightness and excellent output stability. The ASE light source is the combination of high intensity like laser and broad spectrum such as LED. The light is generated inside the core of the optical fiber, and it can be incident on the single mode fiber with low loss coupling. It is an apt equipment for high accuracy measurement applications due to its stable output. The ASE light source is the best source for FBG sensors.

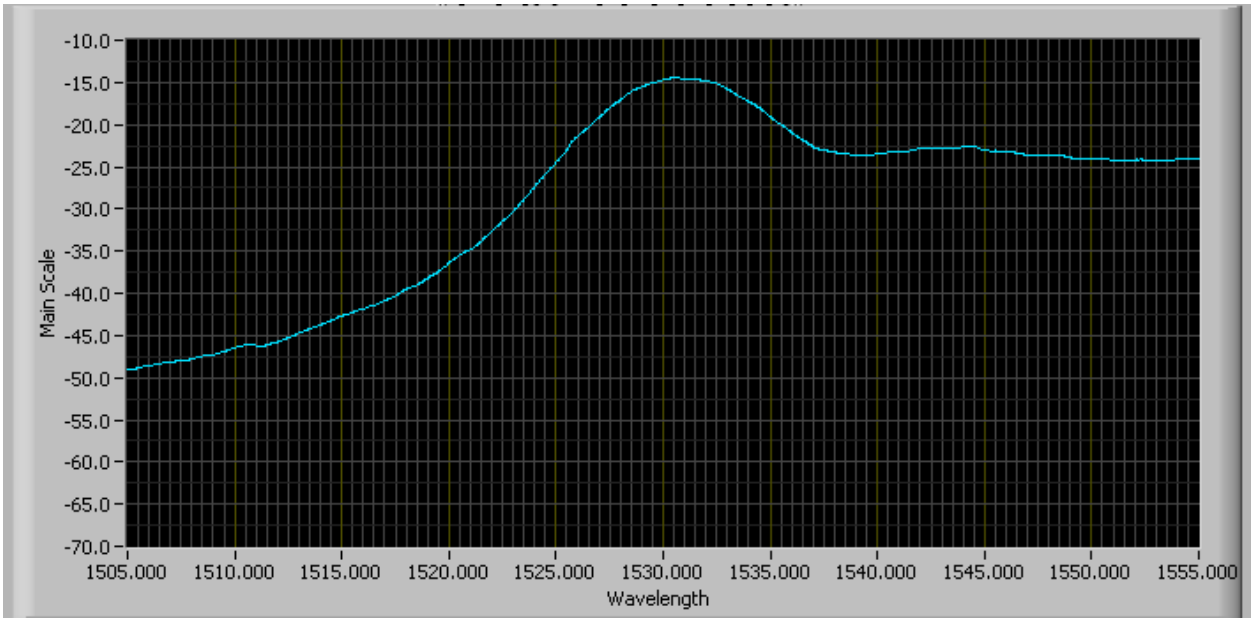

Figure 4-1 Amplified spontanneous emissionn spectrum.

4.1 Principle of ASE Light Source

Amplified spontaneous emission or super-luminescence is light, produced by large fraction of atoms raised to the upper level in the optically dense medium [36]. Active fibers are optical fibers, which not only guide the light, but also they can provide the laser amplification. To achieve this,

the fiber core may have loaded with rare earth ions. The operation principle is the light pump along the fiber that loaded with rare earth ions. If the pumped light has the wavelength shorter than that could transmit along the fiber, then the pump light may absorb by active-laser ions. These are excited into some metastable states. As it is shown in Figure 4-2 the rare earth ions can absorb the pump light then emit it at different wavelength. This emission is called spontaneous emission. Although it is weak, it can trigger the other strong emission. When the intensity of the pumped light is strong enough, the excited ions can now amplify the signal via stimulated emission process. The stimulated emission is happened in the situation which the number of electros in the excited stated exceed from that of in the ground state. Figure 4-3 schematically shows spontaneous emission and stimulated emission. Just like fiber laser and optical fiber amplifier, the ASE light source utilize the stimulated emission.

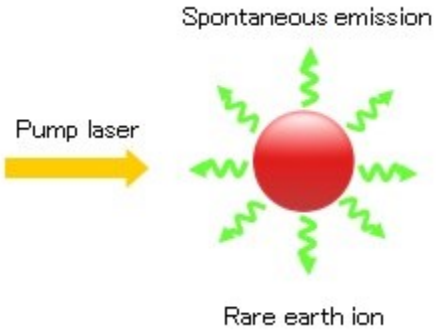

Figure 4-2 the rare earth ions can emit the light at different wavelength from the pump light [37].

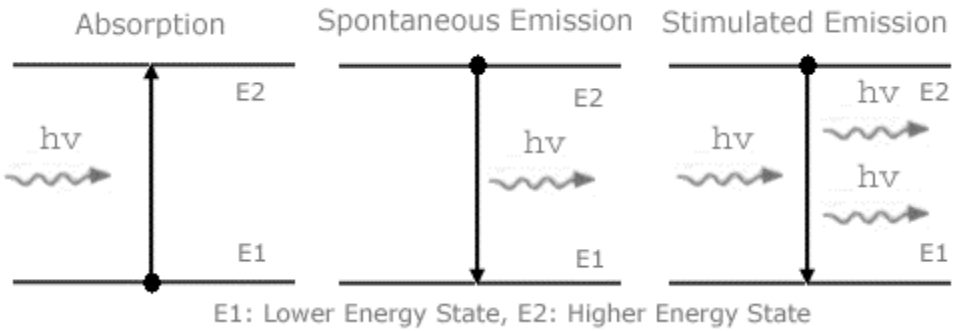

Figure 4-3 Three different process during the interaction of light with matter [36].

As it is mentioned in previous section, only the existence of extremely strong pumped light can cause the stimulated emission. However, if the pump light is confined within the narrow core of the optical fiber then it is plausible to have the high optical power density inside the fiber core. Therefore, by using the rare earth doped optical fiber it is achievable to have stimulated emission in fiber laser, optical fiber amplifier, and ASE light source.

The output of the ASE light source could be the strong light; due to the spontaneous emission light is amplified during the light pass along the fiber. The simultaneous emission happens along the fiber one after another because the strong pump light is existing along the longitudinal direction of the fiber. As it is shown in Figure 4-4, the output light from the ASE light source is strong as the light passes through the fiber.

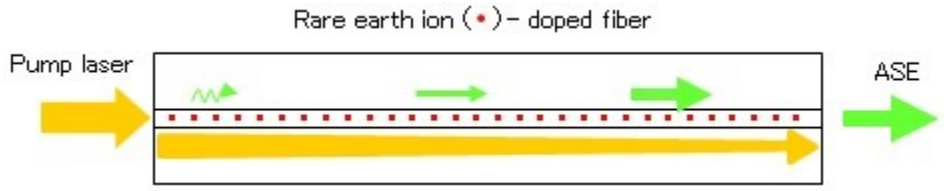

Figure 4-4 The spontaneous emission is amplified by stimulated emission as the light passes through the fiber core [37].

Two factors have influence on the wavelengths of the emitted light from the ASE light source. The first factor is the kind of the rare earth ions that is used as a dopant, and the other factor is type of the fiber and optical fiber material. Each kind of the rare earth ion emits the light at specific wavelength correspond to the energy band diagram of the elements. The difference that is caused by fiber materials is based on how fast the energy of the excited electron can turn to thermal energy in the fiber. As an example, the emission wavelengths for the fluoride fiber is higher than the silica fiber, due to the ratio of conversion into the thermal energy is smaller in a fluoride fiber.

The other distinctive feature of the fluoride fiber is its capability to light emission at shorter wavelength than that of is pumped. The reason is due to as the electron is excited into first excited state it is probable to excite to the second excited state.

4.2 ASE light source spectrum analysis

Figure 4-1 is the output spectrum of ASE light source. The ASE light source is chosen for our experiment is ASE-C band light spectrum without gain flattening filter (GFF). We just want to find the linear part in the input spectrum in order to set our sensor in that range. It is possible to use 1532nm -1538nm range and FBG with Bragg wavelength at 1534nm. In range of 1534nm to 1538nm, it is 4nm range; it is possible to detect temperature for around 400^0C range. Reflectivity would be larger 90% of full width half-maximum (FWHM) and any wider FWHM, it is possible to receive more power (the system will receive more power, if you use wider FBG FWHM). In addition, in range of 1525nm -1531nm and FBG with Bragg wavelength at 1528nm, it is 4nm range; it is possible to detect temperature around 400^0C Range. With reflectivity larger than 90% FWHM or with any more widely, the system will receive more power. Total usable bandwidth (BW) is around 6nm or 600 C. power change in this 6nm is around 10 dBm or around 0.017 dBm/C nearly 1.004 mW/C*power factor. The reflectivity which is needed for my annealing process and system reflect power need higher FBG reflectivity. Higher FBG reflectivity will affect/reduce to the FBG strength (pulling testing).

As it is possible to see in the spectrum, the behavior of the light source in some range of wavelength is linear. Finding the linearity in the ASE light source spectrum that is the input light source of the designed temperature sensor can help us prove our hypothesis about the new interrogation method.

Our hypothesis is based on the amplitude modulation of the Bragg wavelength. Many of previous works are done in the field of FBG based temperature sensors, based on frequency modulation of

the Bragg wavelength. Although our introduced method decreases the price and the size of the temperature sensor, it has all of the advantages regarding the fiber Bragg gratings based temperature sensors.

As it is clear in the Figure 4-1, part of the spectrum, which has the wavelength approximately between 1523 nm to 1527 nm, has the linearity in relation between amplitude in dBm and wavelength in nm. The linearity relation can be seen for the wavelength between 1533 nm to 1537nm.

The prepared sensors for the experiments have the Bragg wavelength for around 1530 nm, so we tried to find the linearity in this range of the wavelength. By using Matlab Simulink, we found the proper linearity in ASE light spectrum in a wavelength range of 1533 nm to 1537 nm. Figure 4-5 shows the Matlab result of the analysis of spectrum. As clearly is shown in figure there is a good response of linearity exist for the ASE light source.

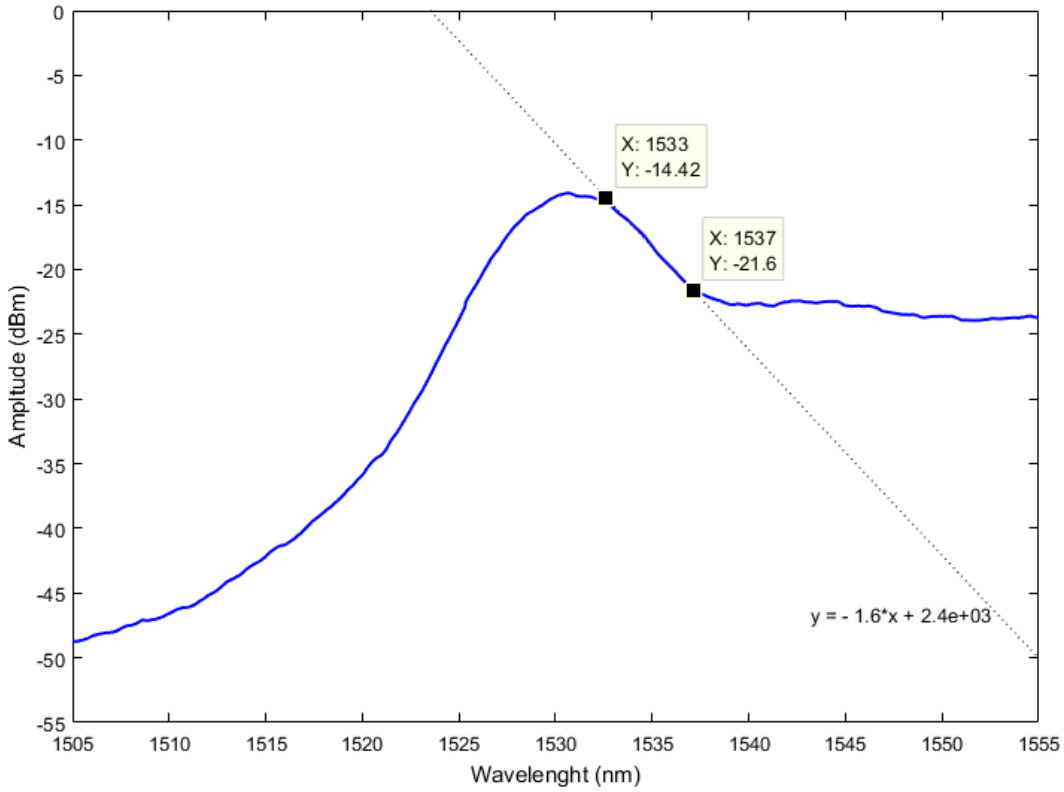

Figure 4-5 The analysis of the ASE light source spectrum. The spectrum of LED and EDFA light source.

In addition, finding the linearity process has repeated for the other ASE light sources, which were available in the laboratory. Two other ASE light sources have been studied in addition to the one that have discussed in previous sections. In compare with the ASE light source, which was selected for our FBG temperature sensor, the following two are also C-band light spectrum without GFF, but with lower power in compare with the one that we decided to use. The point of studying other ASE light source is, in case of emergency when the input designed light source faces some problem, is it possible to change the light source with other available ASE light sources. The answer is provided in the following.

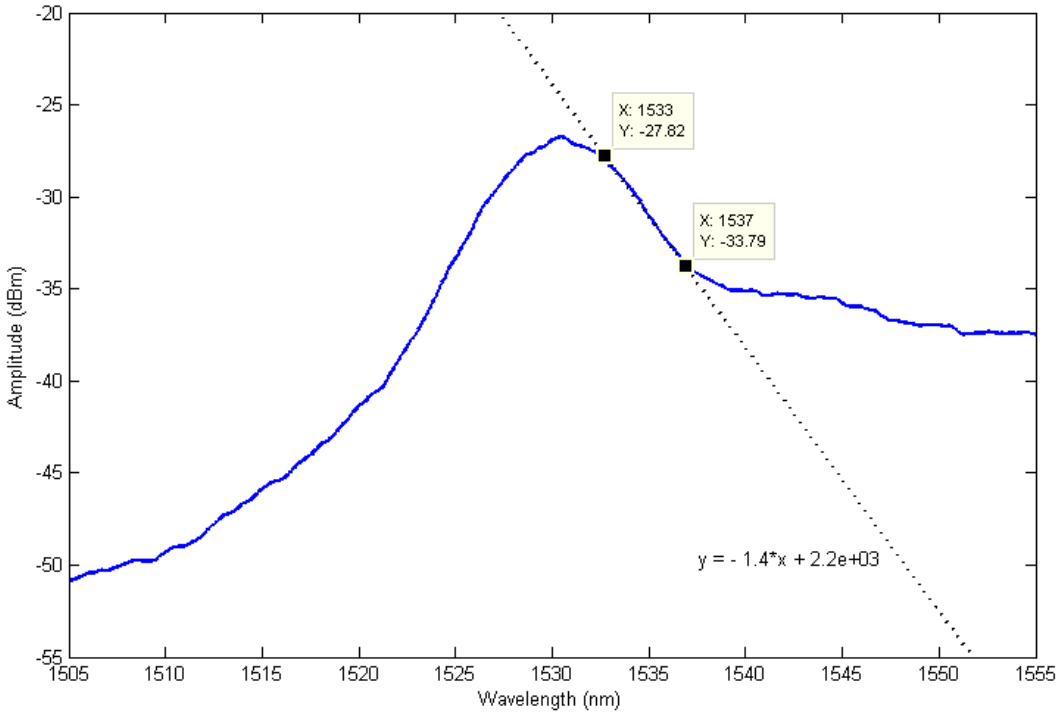

Figure 4-6 The analysis of the ASE light source spctrum. The spectrum of EDFA light source.

Figure 4-6 is the second ASE light source that can be used as an alternative for the original ASE light source. The difference between these two sources is the original source is erbium-doped fiber amplifier (EDFA) which fed with light emitting diode (LED). The second light source is EDFA itself without any source for amplification. As it is clear in figure, the power of this ASE light source is lower than the one with LED and EDFA. The power in this respect is important for our design, because the designed temperature sensor has many connections and each connector has around 0.3 dB loss. It is possible to find the linearity at the same wavelength like the other ASE light source. The range of wavelength is 1533 nm to 1537 nm; it is 4 nm ling which is suitable for detection of temperature changes around 400 ^{0}C. In this range, the change in the amplitude is around 6 dBm for both of the ASE light sources.

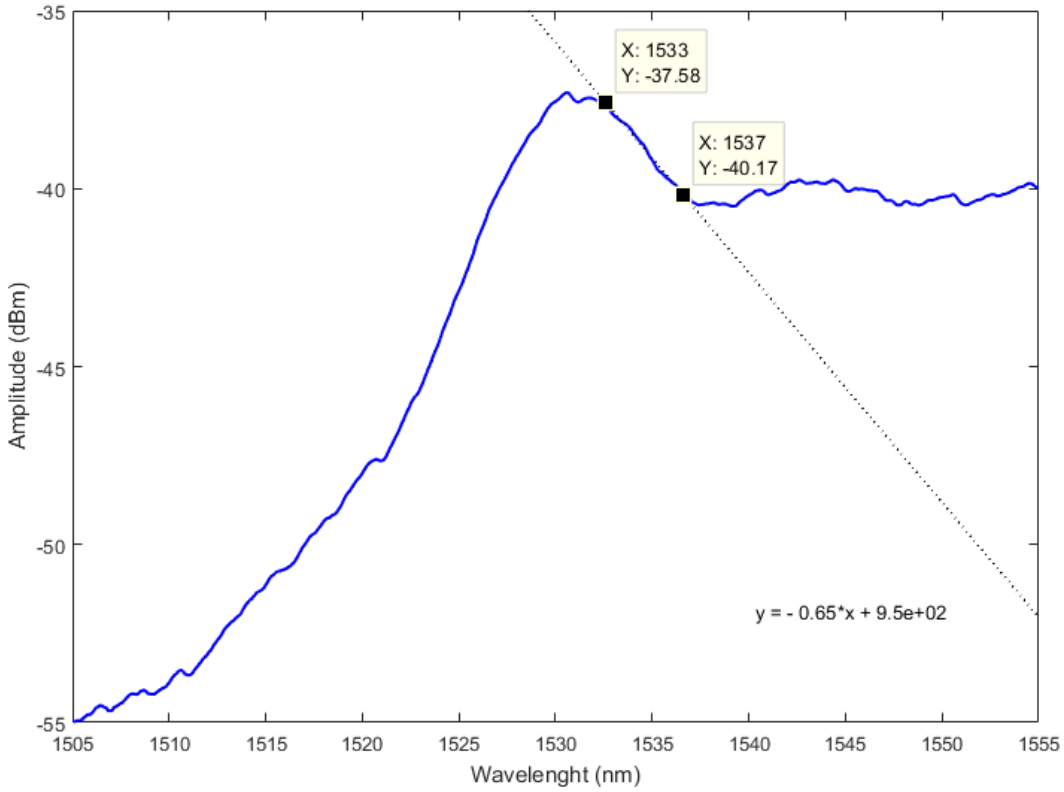

Figure 4-7 The analysis of the ASE light source spectrum. The spectrum of LED light source.

Figure 4-7 shows another available light source. The power of that is low as -37 dBm in the peak, which cannot give us good signal in the output and the signal is more like noise. Therefore, by studying this light source we can consider it as useless for our experiment.

5 The Bragg Wavelength Analysis and Long Term Stability Testing

The aspect that make the Bragg wavelength desirable for sensors is its specific characteristics. In practice, the strain and temperature have direct effect on effective refractive index of the core and the spatial periodicity of the grating. Specially, the effective refractive index is modified through the thermo-optic and strain-optic effects, respectively[38]. We saw from equation 2-3, that when an FBG exposed to any strain variation,$\Delta\varepsilon$, or temperature perturbation, ΔT, it results in the shift in the Bragg wavelength, $\Delta\lambda_B$, which is given by:

$$\Delta\lambda_B = 2\left(\Lambda\frac{dn_{eff}}{dT} + n_{eff}\frac{d\Lambda}{dT}\right)\Delta T + 2(\Lambda\frac{dn_{eff}}{d\varepsilon} + n_{eff}\frac{d\Lambda}{d\varepsilon})\Delta\varepsilon \quad \textit{Equation 5-1}$$

In Equation 5-1, the first term shows the effect of temperature on the Bragg wavelength. The shift in the Bragg wavelength due to the thermal expansion originally comes from the modification of the grating spacing and the refractive index. It is possible to deduct from Equation 5-1, the relative wavelength shifts due to the temperature change ΔT as following:

$$\frac{\Delta\lambda_B}{\Delta T} = \lambda_B\left(\frac{1}{n_{eff}}\frac{dn_{eff}}{dT} + \frac{1}{\Lambda}\frac{d\Lambda}{dT}\right) \quad \textit{Equation 5-2}$$

Where the term $\frac{1}{n_{eff}}\frac{dn_{eff}}{dT}$in Equation 5-2 is the thermo-optic coefficient, which has the value of $8.6 * 10^{-6}\ K^{-1}$ for the germanium doped silica core optical fiber and the term $\frac{1}{\Lambda}\frac{d\Lambda}{dT}$ is the thermal expansion coefficient with approximate value equal to $0.55 * 10^{-6}\ K^{-1}$ for silica optical fiber. In telecommunication systems the wavelengths near room temperature, λ_B varies with temperature at approximately 10 pm/°C [39]. The second term of the Equation 5-1 is not considered in this study as during the experiment the applied strain was taken as zero. Thus, the second term is zero in our experiment.

5.1 Initial Data of the Sensor Head

In the previous works, the interrogation system of the sensors was based on the detection of the Bragg wavelength and its shifts due to the change in temperature or strain. Most of the interrogation system have optical spectrum analyzer (OSA) in their design. OSA has its own limitation in response time, resolution, weight, size, and cost. To overcome these issues, we developed the distinctive interrogation technique. In our design, we tried to relate the Bragg amplitude change to the change in the temperature. This method can solve the problems regarding the high price and big volume of the previous optical sensors. The configuration of the designed senor is shown in chapter 3. Prior to setup the high temperature sensor based on FBG as shown in Figure 3-4, we needed to prepare the sensor head. Consequently, for the experiment, we prepared two sensor heads.

On the subject of sensor head, one off the sensor head has Bragg wavelength at 1549.7 nm and the other prepared sensor head has the Bragg wavelength at 1529.55 nm. In this part each of the sensor heads will be analyzed in the initial circumstances.

In order to fabricate the sensor head, first, with stripper we strip one of the end of fiber Bragg grating and the APC connector. Then with cleaver, we cut the end of the fiber Bragg grating and the APC connector. Cleaver is a device in an optical fiber for deliberate, controlled break, intended to create a perfectly flat end face, perpendicular to the longitudinal axis of the fiber. This process makes an optical fiber ready for fiber splice operation, either fusion splice or mechanical splice.

Later, in order to splice the fiber Bragg grating with APC connector, we use the fusion splice device for splicing. Figure 5-1 (a) shows the prepared sensor head for our experiment.

As the sensor head is prepared, for testing the FBG sensor head, we need to setup the system as shown in Figure 3-1. By simulation the system with LabVIEW software, it makes possible for us to save the data of the Bragg wavelength. We export the data of the FBG return signal (the

wavelength and the amplitude of the signal) and plot them with Excel. The configuration of the system is shown in Figure 5-1 (b).

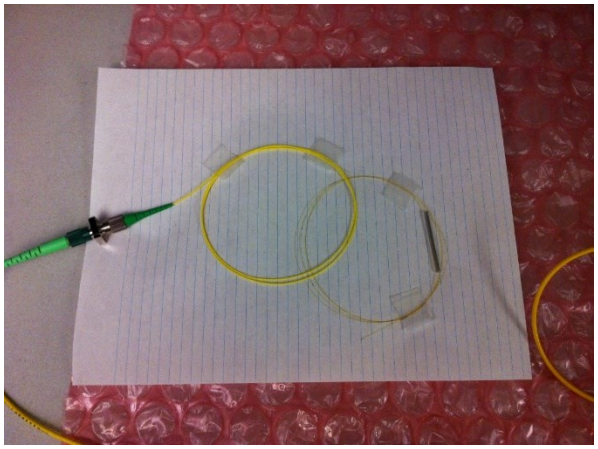

(a)

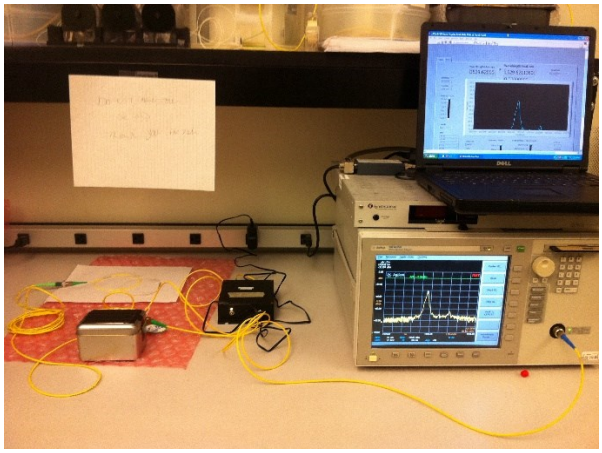

(b)

Figure 5-1 a) The prepared sensor head with Bragg grating at 1549.7 nm. b) The system configuration for FBG testing.

The next step after preparing the sensor head and setup the system is calibration. The sensor head is tested in initial and harsh situation and compare all the result with the reference point. The initial experiment starts with the sensor head with Bragg wavelength at 1549.7 nm. At room temperature, the Bragg wavelength at 1549.7 nm has the amplitude of -36.4 dBm. The Bragg wavelength at room temperature is shown in Figure 5-2. This figure is recorded after the fabrication of the fiber Bragg grating.

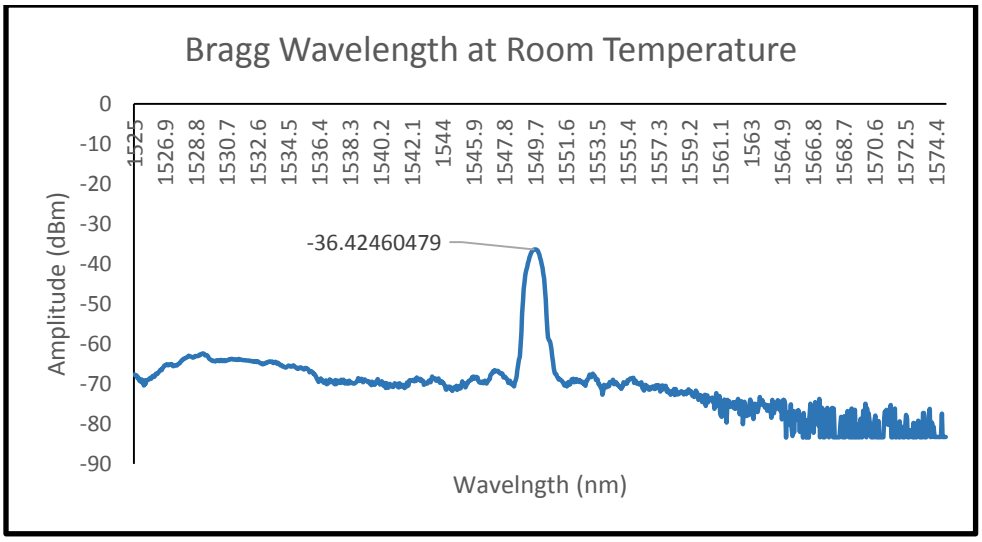

Figure 5-2 The return signal of the FBG sensor head with Bragg wavelength at 1549.7 nm at room temperature.

During the experiment, especially for long-term stability testing, we choose 0°C as a reference temperature. In order to test the FBG sensor head we put the sensor head inside the mixture of ice and water after each step. For starting, the initial result of the first sensor head at 0 °C is shown in Figure 5-3. This figure is used as a reference check the stability of the sensor during the high temperature.

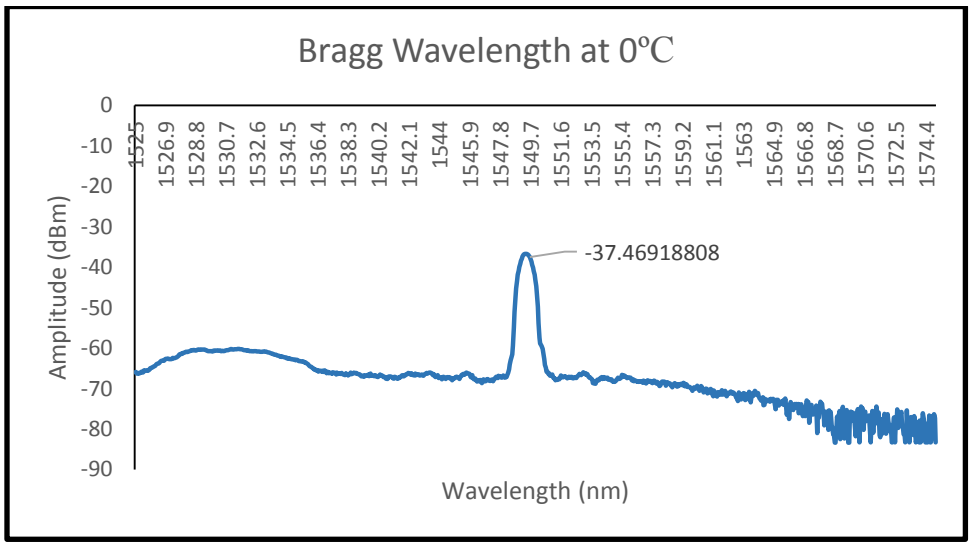

Figure 5-3 The return signal of the FBG sensor head with Bragg wavelength at 1549.7 nm at 0°C.

Two senor head is prepared for our experiment, as mentioned before. The backward FBG spectrum of the one with 1549.7 nm Bragg wavelength is discussed above. In the following, the return signal of the FBG with Bragg wavelength at 1529.55 at room temperature (Figure 5-4) and 0 ºC (Figure 5-5) is shown.

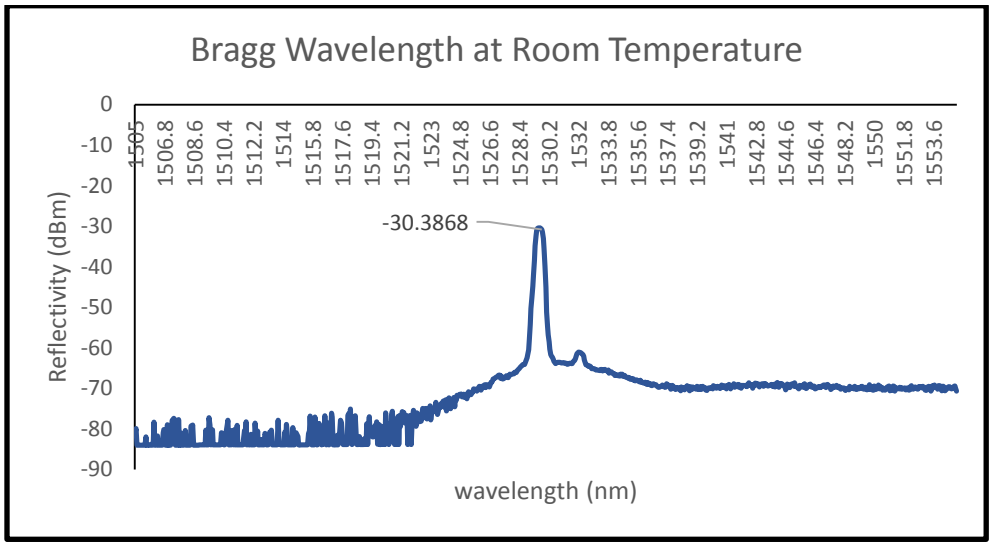

Figure 5-4 Fiber Bragg grating backward reflected light with the Bragg wavelenngth at 1529.55 nm at room tempearture.

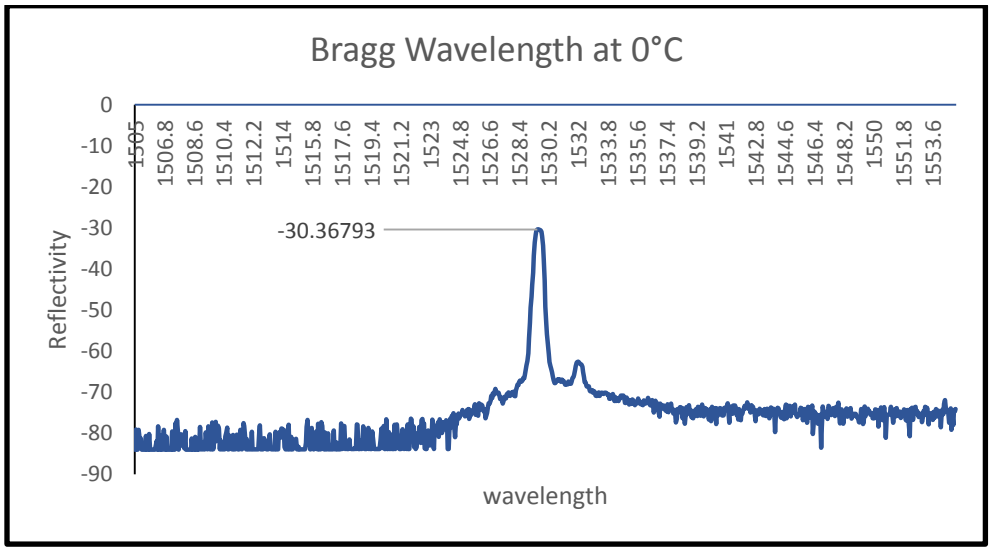

Figure 5-5 The return signal of the FBG with Bragg wavelength at 1529.55 nm at 0 °C.

As shown above, two prepared senor head, in addition to their Bragg wavelength they have different amplitude for their return signal. The sensor head with Bragg wavelength at 1529.55 nm shows more power in its FBG reflected signal. In addition to intrinsic factor, which mentioned in chapter 0, some factors related to the fabrication have direct impact on the amplitude of the reflected light. As an example, perfectly flat end face of each fiber, clean surface of the fibers before splicing (after striping the fibers and cleave the ends some dust remains on the surface which cause some flaws in the splice and therefore some loss), flawless splicing that means the core of the fibers perfectly aligned before splicing.

5.2 Optical Spectrum Analyzer Calibration

The system we setup for the long-term stability and calibration of the high temperature sensor based on FBG includes optical spectrum analyzer (OSA) as shown in Figure 3-1. OSA is located in the system for detecting the amplitude and the wavelength of reflected light from the FBG. Different OSA calibration may cause different the shape and the amplitude of the output.

One of the factors in OSA calibration that directly influences on the power of the output light is wavelength bandwidth resolution. The bandwidth of the band-pass filter dictates the resolution bandwidth (RBW), which determines the fast Fourier transform (FFT) bin size, or the smallest frequency that can be resolved. The ability of an optical spectrum analyzer to display two signals closely spaced in wavelength as two different responses is determined by the wavelength resolution. The smaller RBW, has much finer resolution which allows the sidebands to be visible.

Bandwidth of the optical filter is determining the wavelength resolution. The key components of the optical filter are monochromator aperture, photodetector fiber, input image size, and the quality of the optical components. The wavelength resolution is specified as the filter bandwidth at half-power level, known as a full width at half maximum. This is the good indication of the optical spectrum analyzer ability to resolve equal amplitude signals.

The optical spectrum analyzer which is used in the experiment is Agilent 86142B have selectable filters of 0.06 nm and 0.1 nm to 10 nm in a 1, 2, 5 sequence, which make it possible to sufficient resolution for most measurements.

In order to find the best wavelength resolution bandwidth for our experiment, we set it to 0.1 nm, 0.5 nm, and 1 nm. Figure 5-7, Figure 5-8, and Figure 5-9 show the result of them respectively. The FBG reflected back light which is shown in Figure 5-4, is the result of automatic setting (mode) for the resolution inside the OSA. The Figure 5-6 is showing the calibration of the OSA which used for the experiment. This figure is the screenshot of the LabVIEW software and the resolution bandwidth is 70×10^{-3}nm.

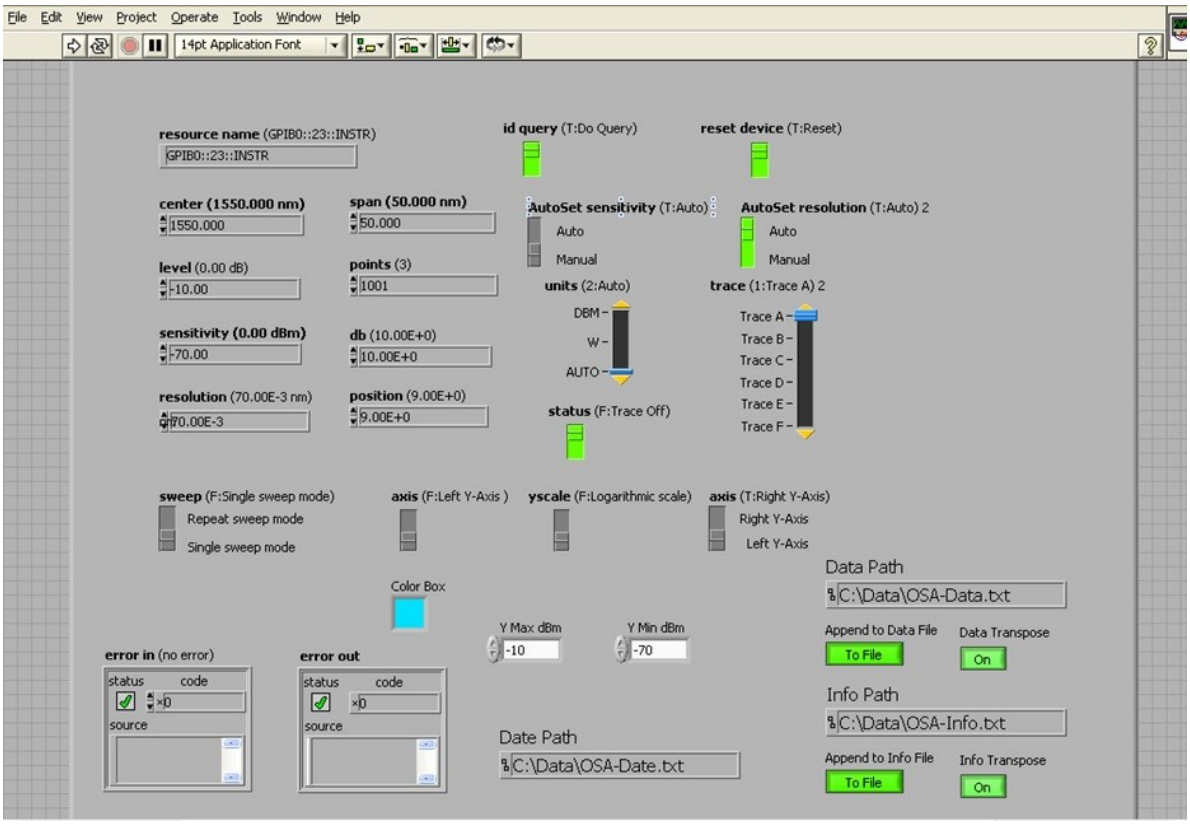

Figure 5-6 screenshot of the OSA setting during the experiment.

Figure 5-7 is showing the result of bandwidth resolution of 0.1 nm. The FBG reflected back spectrum has the sharp peak with amplitude of -30.625 dBm. The amplitude of the output is nearly

the same with for both resolution bandwidths. The shape of the spectrum is nearly the same as well.

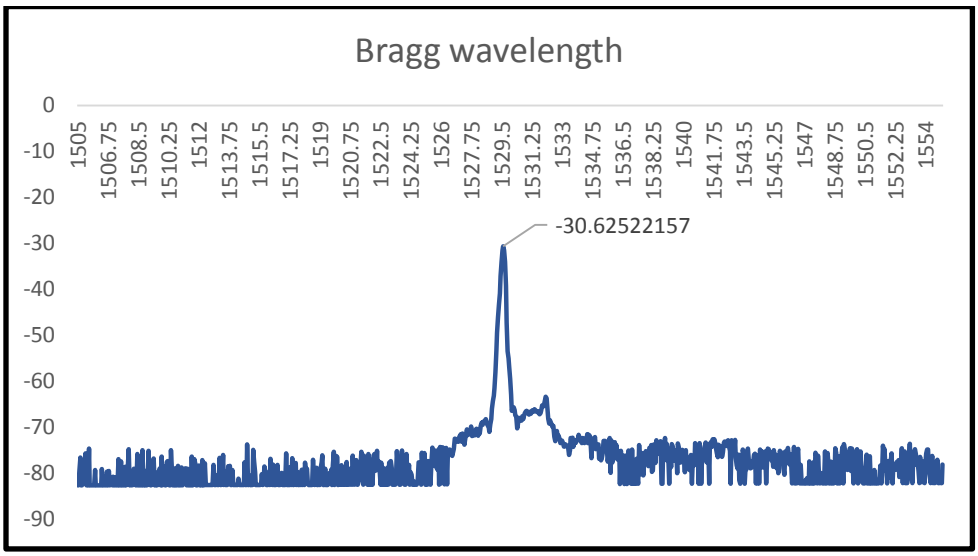

Figure 5-7 The reflected spectrum of the FBG with the Bragg wavelength at 1529.55 nm at room temperature. The wavelength resolution bandwidth of the OSA is set on 0.1 nm for getting this sepctrum.

The figure below (Figure 5-8) is showing the bandwidth of 0.5 nm. As it can be deduced from the figure, the amplitude of the spectrum is increased for about 4 dBm. To compare the shape of this spectrum with the previous ones, we can say that the peak of the spectrum is not as sharp as they were.

Our goal to change the wavelength resolution bandwidth spectrum is to find the in term of amplitude, the strongest FBG reflected-back light. In addition, in term of the shape of the spectrum, we need the sharp peak in order to detect the exact amount of the Bragg wavelength. To consider the factors that mentioned above, setting the resolution bandwidth at 0.5 nm gives the better output than the 70×10^{-3}nm in our experiment.

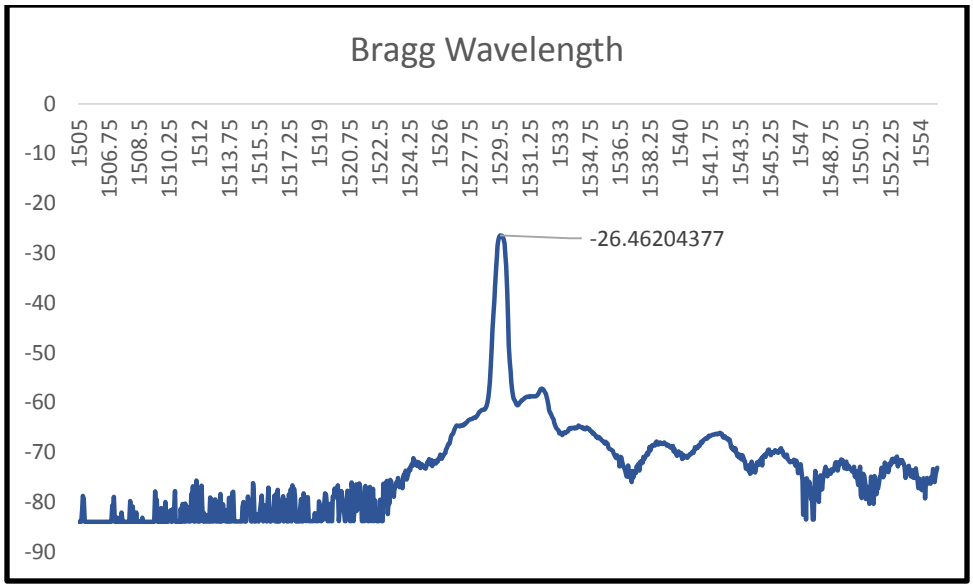

Figure 5-8 The reflected spectrum of the FBG with the Bragg wavelength at 1529.55 nm at room temperature. The wavelength resolution bandwidth of the OSA is set on 0.5 nm for getting this sepctrum.

With the same configuration as it is shown in *Figure 5-1* b, we change the wavelength resolution bandwidth to 1 nm at room temperature for the FBG with Bragg wavelength at 1529.55 nm. Figure 5-9 shows the result of the 1 nm resolution bandwidth. As it is clear in the figure, the spectrum has the flat peak, which is not desirable for our experiment due to we need the exact amount of the Bragg wavelength for our calibration the sensor. The exact amount of the Bragg wavelength cannot be extracted from the spectrum; it can say that the Bragg wavelength is in the range of 1 nm. To compare the amplitude of the FBG back reflected light at wavelength bandwidth resolution of 1 nm and 0.5 nm, it is clear that the amplitude roughly remains the same.

Overall, there is no advantage in increasing the wavelength bandwidth resolution to 1 nm. The good output result for our experiment can be extracted from the resolution bandwidth of 0.5 nm.

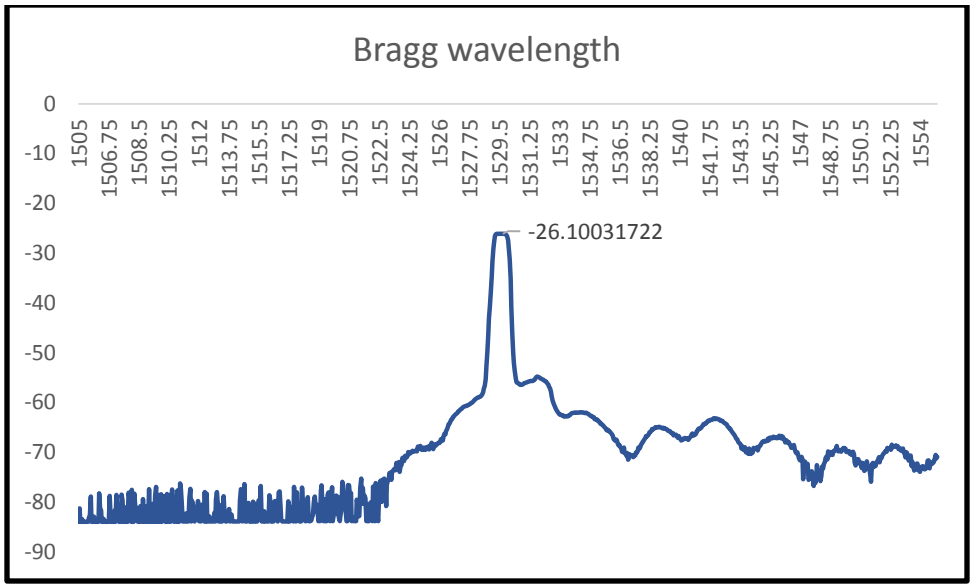

Figure 5-9 The reflected spectrum of the FBG with the Bragg wavelength at 1529.55 nm at room temperature. The wavelength resolution bandwidth of the OSA is set on 1 nm for getting this sepctrum.

5.3 Sensor Calibration

The next phase of our experiment is finding the relation between the shift in the Bragg wavelength and the temperature. We use the configuration of the system interrogation as it is shown in Figure 3-1. At first, the sensor head was kept in the laboratory freezer at 0 °C. We run down the temperature form 0 °C to -27ºC. The result of Bragg wavelength with respect to the temperature is recorded. The reference amount of the Bragg wavelength was set in the 0 °C temperature and we calculated the shift in the Bragg wavelength with respect to amount of the Bragg wavelength at 0 °C.

In addition, we take out the FBG form the freezer and let the FBG to rest for about an hour in order to prevent the breakage of sensor head. At the time when the FBG reach the room temperature, we put the FBG at furnace. We run up the temperature from the room temperature to 400 °C for many times. The Bragg wavelength with respect to temperature is recorded. The shift in the Bragg wavelength was calculated with the reference amount of Bragg wavelength at 0 °C.

The process, which explained above, was repeated on our two prepared sensor head for several times. In the following the result of running up the temperature is shown. The experimental result is compared with the calculated data using the Matlab software. All the data then exported from the Matlab software and plotted using Excel.

$\lambda B \Delta T = \lambda B 1 neff dneff dT + 1 \Lambda d \Lambda dT$ Equation 5-2. The equation for germanium doped silica fiber become

$$\frac{\Delta\lambda_B}{\Delta T} = \lambda_B(8.6 \times 10^{-6} + 0.55 \times 10^{-6}) \quad \textit{Equation 5-3}$$

Where $\Delta\lambda_B$is the shift in the Bragg wavelength, ΔT is the temperature perturbation and $\lambda_B$is the reference Bragg wavelength. During each step, the experimental result was compared with the simulation result.

in addition, we need to examine that during the increment in the temperature, the FBG remains strong. In order to find the strength of the FBG for each set of data we calculate the normalized refractive index change. If the amount of the normalized refractive index change become less than 1, means that the grating start to wash out.

In order to calculate the normalized index of refraction, we use the equation taken from [40]. The refractive index modulation is calculated by equation 5-4, considering the typical confinement factor $\nu = 0.8$

$$\Delta n_{AC} = \frac{\lambda_B . atanh(\sqrt{R})}{\nu . \pi . L} \qquad \textit{Equation 5-4}$$

Where the Δn_{AC}, is the refractive index modulation, λ_B is the Bragg wavelength, R is the reflectivity, and L is the length of the FBG. We calculate the normalized refractive index modulation to make the figures easier to understand.

In the following, Figure 5-10 shows the experimental result of change in the Bragg wavelength with respect to temperature (blue line). The blue dashed line shows the first-degree regression line

with equation of y = 0.009x - 0.0921. In addition, the orange line is the simulation result of the Bragg wavelength shift with respect to temperature for germanium doped silica fiber. In the same way, the orange dashed line is the first-degree regression line with the equation of y = 0.0092x - 1E-05.

As it is clear from the picture and the equations of fist degree, the two data sets do not fit. The slope of the two lines are roughly equal. In some data points the experimental result and the result from the simulation is equal.

Furthermore, Figure 5-10 shows the normalized index of refraction with respect to change in temperature. As it is clearly shown in figure, the effective index of refraction remains strong during testing.

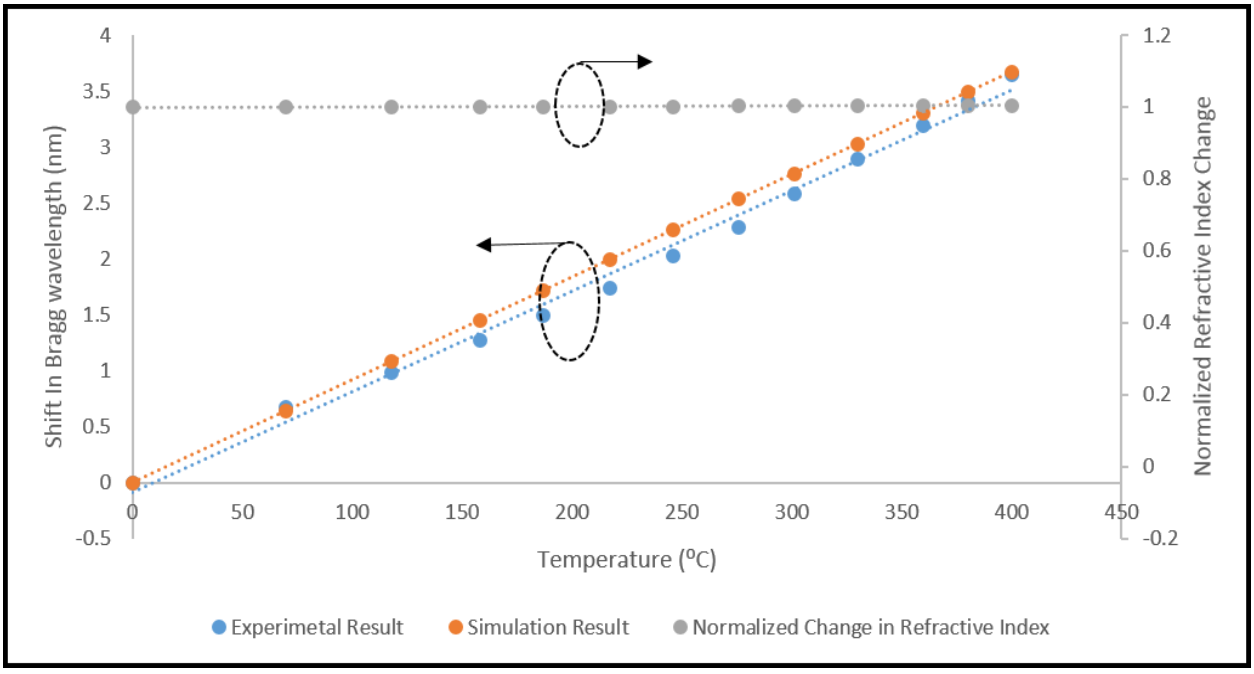

Figure 5-10 Change in the Bragg wavelength with respect to running the temperature up to 400°C from 0 °C in experimental result (blue line), and in simulation (orange line)and their first degree regression line. The normalized refraction index change during the running up the temperature (grey line).

Table 1 Regression table of the data of change in the Bragg wavelength with respect to temperature for sensor head with peak reflection at 1529.55 nm.

SUMMARY OUTPUT								
Regression Statistics								
Multiple R	0.9964							
R Square	0.9928							
Adjusted R	0.9922							
Standard E	0.0987							
Observatio	13.0000							
ANOVA								
	df	*SS*	*MS*	*F*	*Significance F*			
Regression	1.0000	14.8808	14.8808	1527.2971	0.0000			
Residual	11.0000	0.1072	0.0097					
Total	12.0000	14.9880						
	Coefficients	*Standard Error*	*t Stat*	*P-value*	*Lower 95%*	*Upper 95%*	*Lower 95.0%*	*Upper 95.0%*
Intercept	-0.0921	0.0605	-1.5233	0.1559	-0.2252	0.0410	-0.2252	0.0410
X Variable	0.0090	0.0002	39.0806	0.0000	0.0085	0.0095	0.0085	0.0095

The F-Test value represented in the Analysis of Variance (ANOVA) table confirms that the proposed linear relationship is valid. Therefore, there is a statistical ground to correspond dependent variable's variation (Shift in Brag wavelength) to the independent's one.

Coefficient of determination, R^2, explains the degree of variation in dependent variable which can be explained by change in independent variable. The higher the number, the more relation between our data persists. The R^2 value for these set of data is

$$R^2 = 0.9928$$

The above figure is related to prepared sensor head with Bragg wavelength at 1529.55 nm. In the following, the sensor head with Bragg wavelength at 1549.7 nm is tested. Figure 5-11 shows the experimental and simulation result of the shift in Bragg wavelength with respect to change in temperature as well as normalized refractive index change with respect to temperature. The senor head is kept inside the laboratory freezer. The temperature goes down from 0 °C to -27°C. Next, the sensor head is put inside the furnace, and we start to increase the temperature from room temperature to 400 °c. All the data is the saved from the LabVIEW.

The procedure was the same as the sensor head with Bragg wavelength at 1529.55 nm. With experimental result from LabVIEW, the shift in Bragg wavelength with respect to temperature is calculated in accordance with 0 °C result. The shift in Bragg wavelength with respect to temperature is simulated as well. The normalized refractive index change is simulated with Matlab.

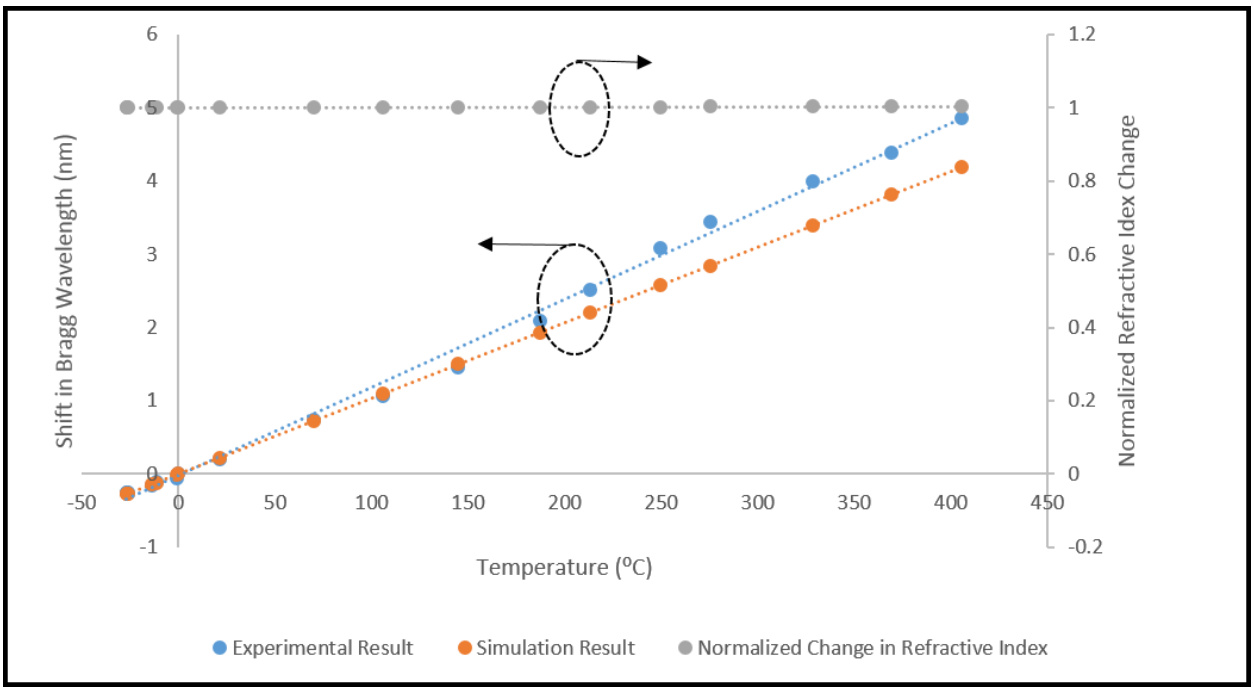

Figure 5-11 Change in the Bragg wavelength with respect to running the temperature up to 400°C from -27 °C in experimental result (blue line), and in simulation (orange line)and their first degree regression line. The normalized refraction index change during the running up the temperature (grey line).

As a result of Figure 5-11, the sensor head which is used in this experiment, fiber Bragg grating Corning SMF-28, Ge-doped optical fibers with 4% Ge content in its core and it is loaded with hydrogen prior to writing with 248 nm excimer laser, remains strong during the increasing the temperature to 400 °C; due to the normalized refractive index change during the experiment remains at 1.

Table 2 Regression table of the data set of change in the Bragg wavelength with respect to temperature for sensor head with peak reflection at 1549.7 nm

SUMMARY OUTPUT								
Regression Statistics								
Multiple R	0.9982							
R Square	0.9965							
Adjusted R Square	0.9962							
Standard Error	9.2048							
Observations	18.0000							
ANOVA								
	df	*SS*	*MS*	*F*	*Significance F*			
Regression	1.0000	380731.2469	380731.2469	4493.5611	0.0000			
Residual	16.0000	1355.6508	84.7282					
Total	17.0000	382086.8978						
	Coefficients	*Standard Error*	*t Stat*	*P-value*	*Lower 95%*	*Upper 95%*	*Lower 99.0%*	*Upper 99.0%*
Intercept	2.7363	2.8420	0.9628	0.3500	-3.2884	8.7611	-5.5644	11.0371
X Variable 1	82.9692	1.2377	67.0340	0.0000	80.3454	85.5930	79.3541	86.5843

Coefficient of determination, R^2, is calculated for the data point of change in the Bragg wavelength with respect to temperature for sensor head with Bragg wavelength at 1549.7 nm. The R^2 value for these set of data is

$$R^2 = 0.9965$$

5.4 Long-term Stability Testing

In previous chapters, we introduced our idea. The idea is instead of temperature sensor interrogation system based on wavelength modulation, we use the interrogation system based on amplitude modulation. For our experiment we focus on the reflectivity of the sensor head as the temperature changes.

In previous section, we investigate the linear relation between Bragg wavelength change and the temperature. Afterwards, we need to test the sensor head in harsh situation where the sensor head utilized for detecting the high temperature, 400 °C as an example, for several hours or temperature goes higher than 400 °C.

For achieving this goal, we design the experiment. We put the sensor head with Bragg wavelength at 1549.7 nm at furnace with temperature of 400 °C for 338 hours. Then, we brought the sensor head out of the furnace and kept it at room temperature for 4-5 hours. Next, we put the sensor head inside the mixture of water and ice with temperature of 0 °C. We recorded the FBG reflected back spectrum. As mentioned before, in every stage of our experiment, we compare the attained result with the result from 0 °C in initial situation.

Figure 5-12 shows the FBG back reflected light at 0 °C after keep the sensor head with Bragg wavelength at 1549.7 nm at furnace for 338 hours (blue line). In addition, the result is compared with the FBG reflected back spectrum at 0 °C in initial situation (orange line). The figure clearly shows that, there is a drop in reflectivity after 338 hours annealing at 400 °C for less than 3 dBm. This result shows that over the long time usage of the sensor at 400 °C the amplitude of the FBG back reflected light decrease a little, the system based on amplitude modulation is trustworthy.

For long-term stability testing of high temperature senor head, with setup in Figure 5-1 (b), we kept the sensor head with Bragg wavelength at 1549.7 nm inside the furnace for 18 hours at 600 °C. Then, we brought out the sensor head at room temperature and let it rest for some hours. Next, we put the sensor head inside the mixture of ice and water with temperature of 0 °C and record the FBG back reflected light.

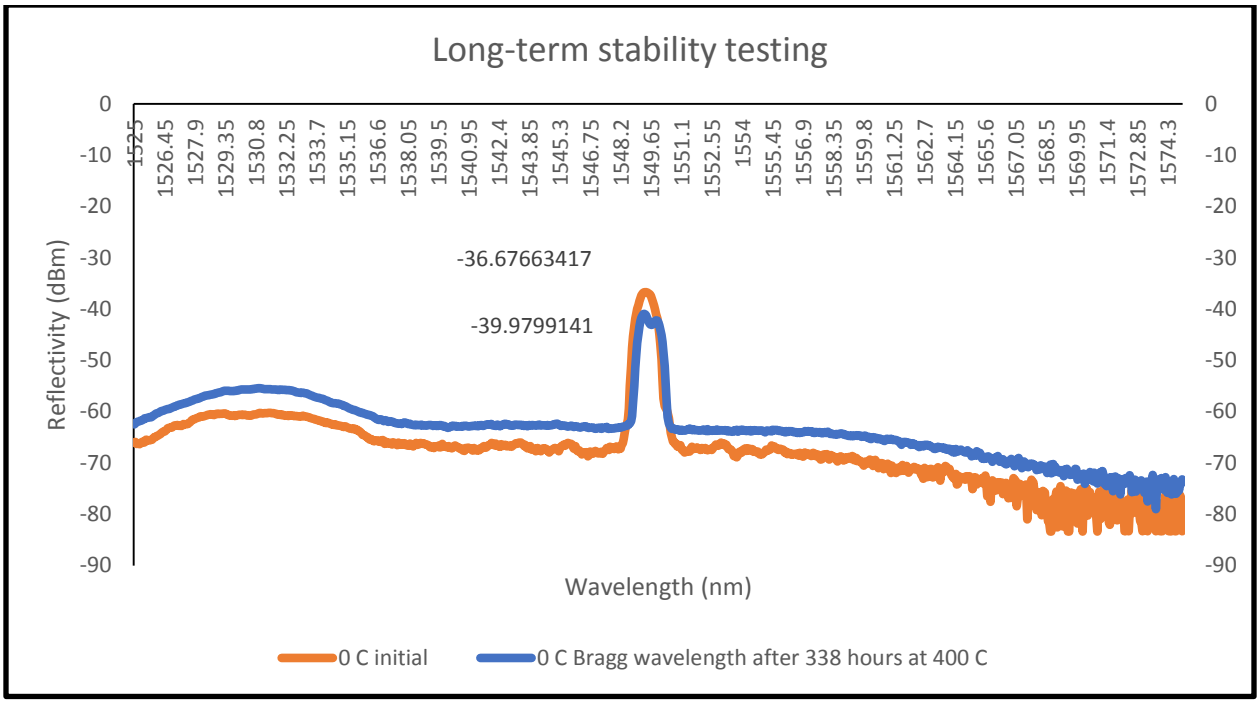

Figure 5-12 The FBG back reflected light at 0°C after 338 hours annealing at 400 °C (blue line) and the FBG back reflected spctrum at 0 °C before annealing (orange line) in sensor head with Bragg wavelength at 1549.7 nm.

Figure 5-13 shows the FBG back reflected spectrum after kept at furnace for 18 hours at 600 °C. the result is compared with the FBG back reflected spectrum at 0 °C before annealing the senor head.

We acclaimed that our high temperature senor based on fiber Bragg grating is good for the temperature between -27 °C to 400 °C. we operate this experiment to show that, in the case when the ambient temperature goes above the limit temperature (400 °C) accidentally, the senor head can tolerate. After annealing, the reflectivity of the sensor head drops for less than 5 dBm about 4.69 dBm in compare with the senor head before annealing.

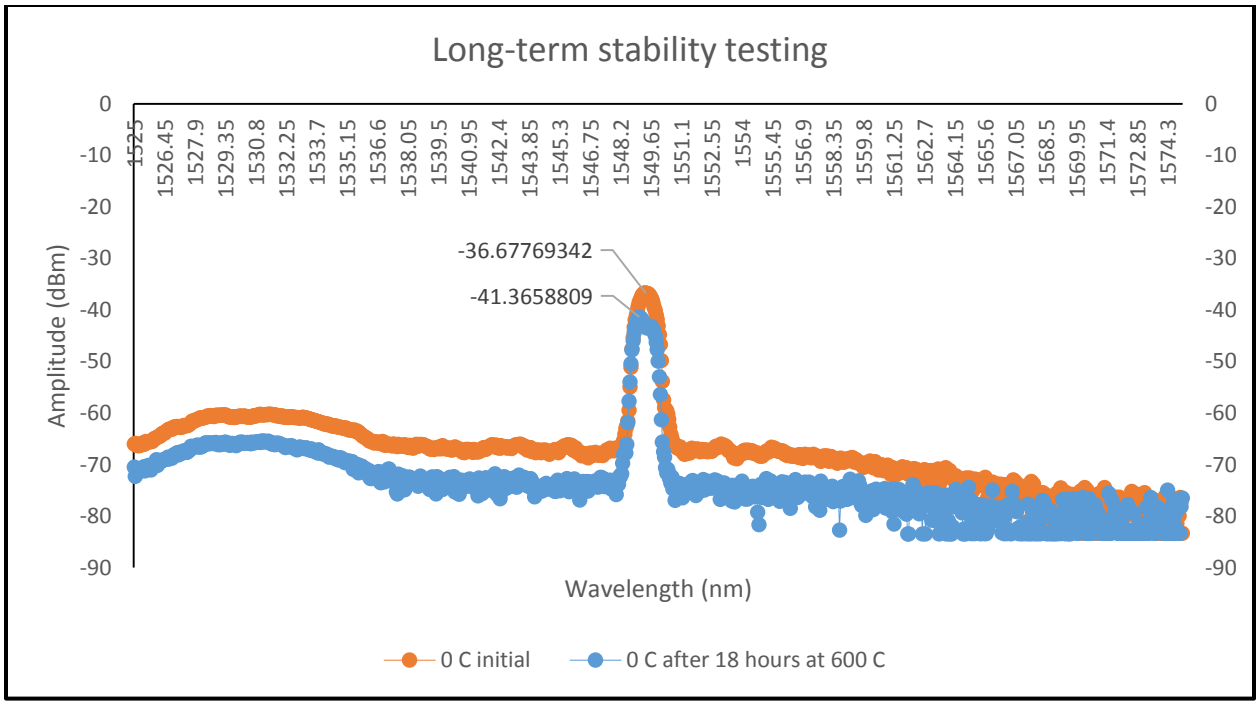

Figure 5-13 The FBG back reflected light at 0°C after 18 hours annealing at 600°C (blue line) and the FBG back reflected spctrum at 0 °C before annealing (orange line) in sensor head with Bragg wavelength at 1549.7 nm.

The last part of the experiment relates to drift in reflectivity. As was previously stated the introduced interrogation system is based on amplitude modulation. In every steps of the experiment we try to keep eye on the change in the amplitude of the FBG back reflected light. In this section we investigate the drop in the reflectivity of the sensor head with Bragg wavelength at 1549.7 nm at 600 °C. Figure 5-14 shows the reflectivity drift at 600 °C for 2000 seconds.

In according to the figure, the zero instant shows the FBG back reflected light at room temperature. As the FBG is put inside the furnace, the FBG beck reflected light amplitude drops to -41.329 dBm. The reflectivity continues to drop gradually as the time passes. After 2000 seconds, kept at 600 °C temperature the reflectivity reaches the -42.896 dBm. During the 2000 seconds the total drift in reflectivity for sensor head with Bragg wavelength at 1549.7 nm is 1.567 dBm.

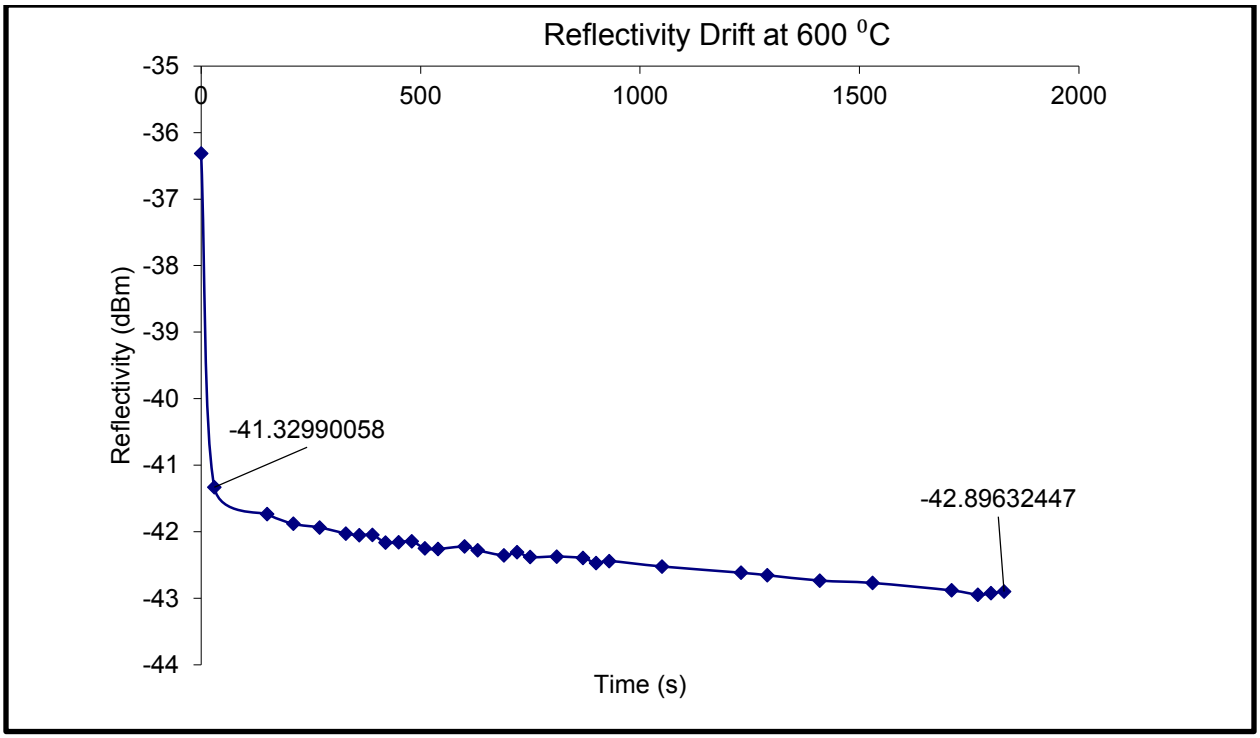

Figure 5-14 the sensor head reflectivity drift at 600 °C for 2000 seconds with Bragg wavelength at 1549.7 nm.

6 Conclusion, contributions and future works

6.1 Summary of Thesis

A high temperature sensor based on Fiber Bragg grating was designed, developed, and characterized. This study introduces the new interrogation system which making the sensor suitable for power transformer. The distinctive characteristics of the designed temperature sensor is, its real-time monitoring, small size, and low cost.

The sensor head that is used in this investigation, is fiber Bragg grating Corning SMF-28, Ge-doped optical fibers with 4% Ge content in its core. It was loaded with hydrogen prior to writing with 248 nm excimer laser. The Bragg wavelength of the two sensors prepared in this work is at 1529.55 nm and 1549.7 nm respectively.

In this study, we need used amplified spontaneous emission (ASE) light source in order to achieve the linear input light for the designed sensors. The sensors head should has Bragg wavelength in the range in which the ASE light source spectrum is linear in this design. In designed sensor, The Bragg reflected spectrum power is converted into its equivalent current with use of photodiode (PD).

In this work, the designed sensor is tested for temperature ranging from -27 ºC to 400 ºC. For testing the stability and reliability of the designed sensors, the sensor head was left inside the furnace at 400°C for 338 hours. Furthermore, the sensor head is tested in 600 ºC for about 18 hours.

Following points are the main achievement of the thesis:

- The new high temperature senor based on FBG is designed, developed, and tested.
- In contrast with existing interrogation methods for FBG based temperature sensors, our design sensor is based on amplitude of the fiber Bragg grating reflected spectrum.

- The ASE light source spectrum is analyzed with Matlab in order work to find the linear range in its spectrum.
- The relation between change in the Bragg wavelength with respect to the temperature is recorded precisely with use of LabVIEW software. As shown in figures, the sensor head shows a linear response in two four nm wide ranges.
- Although the designed sensor is designed for temperature in the range of -27 ^{0}C to 400 ^{0}C, the sensor head shows good stability response for temperature up to 600 ^{0}C for 18 hours.

6.2 Suggestion for Future Work

The two sensor head prepared in this research have the Bragg wavelength at 1529.55 nm and 1549.7 nm. We acclaimed that there are two ranges in the ASE light source that shows the linear response; 1523-1527 nm, and 1533-1537 nm. The sensor heads prepared in this experiment is out of these two ranges. For future work on this field, my suggestion is to prepare two sensor heads with Bragg wavelength at 1523 nm and 1533 nm at room temperature.

The working range of the two new sensor heads would be from room temperature to 400 °C due to the linearity range in ASE light source spectrum is 4 nm (the shift in Bragg wavelength is about 10 pm/°C)

7 References

[1] B. D. Gupta, *Fiber optic sensors: principles and applications*. New India Publishing, 2006.

[2] and D. P. F. Franklin, Arthur Charles, *The J & P transformer book: a practical technology of the power transformer*. Elsevier, 2013.

[3] J. H. Harlow, *Electric power transformer engineering*. CRC press, 2004.

[4] "BREAKING NEWS: Redmond Substation Fire - NBC Right Now/KNDO/KNDU Tri-Cities, Yakima, WA |." [Online]. Available: http://www.nbcrightnow.com/story/14924340/copy-copy-copy-copy-copy-copy-only-breaking-news-with-live-streaming-video. [Accessed: 25-Apr-2016].

[5] G. W. regay, "Optical fiber temperature sensor," U.S. Patent No. 4,794,619., 1986.

[6] K. Hogari, Y. Yamada, and K. Toge, "Novel optical fiber cables with ultrahigh density," *J. Light. Technol.*, vol. 26, no. 17, pp. 3104–3109, 2008.

[7] R. Kashyap, *Fibre Bragg Gratings*. Academic Press, 2010.

[8] H. Kawazoe, "Effect of modes of glass-formation on structure of intrinsic or photon induced defects centered on III, IV or V cations in oxide glasses," *J. Non. Cryst. Solids*, vol. 71, no. 1–3, pp. 231–243, 1985.

[9] B. Lee, "Review of the present status of optical fiber sensors," *Opt. Fiber Technol.*, vol. 9, no. 2, pp. 57–79, Apr. 2003.

[10] M. Zhang, Bowei; Kahrizi, "High temperature resistance temperature sensor based on hydrogen loaded fiber bargg garting," vol. 33, no. 0. p. 2500, 2005.

[11] A. Othonos, "Fiber Bragg gratings," *Rev. Sci. Instrum.*, vol. 68, no. 12, p. 4309, 1997.

[12] A. Othonos, K. Kalli, D. Pureur, and A. Mugnier, "Fibre bragg gratings," *Wavel. Filters Fibre ...*, 2006.

[13] M. Fokine and M. Fokine, *Photosensitivity , chemical composition gratings , and optical fiber based components*. 2002.

[14] D. K. Lam and B. K. Garside, “Characterization of single-mode optical fiber filters.,” *Applied optics*, vol. 20, no. 3. pp. 440–445, 1981.

[15] L. Dong, J. Cruz, L. Reekie, M. Xu, and D. Payne, “Large Photo-Induced Index Changes in Sn-codoped Germanosilicate Fibres-*" P’Ca-S,” 1995.

[16] K. O. Hill and G. Meltz, “Fiber Bragg grating technology fundamentals and overview,” *J. Light. Technol.*, vol. 15, no. 8, pp. 1263–1276, 1997.

[17] K. O. Hill, B. Malo, F. Bilodeau, D. C. Johnson, J. Albert, and K. Hill, “Bragg gratings fabricated in monomode photosensitive optical fiber by UV exposure through a phase mask Bragg gratings fabricated in monomode by UV exposure through a phase mask photosensitive optical fiber,” vol. 1035, no. 1993, pp. 1035–1037, 2005.

[18] R. Article and Y.-J. Rao, “In-fibre Bragg grating sensors,” *Meas. Sci. Technol.*, vol. 8, no. 4, pp. 355–375, 1997.

[19] K. O. Hill, “Photosensitivity in optical fiber waveguides: From discovery to commercialization,” *IEEE J. Sel. Top. Quantum Electron.*, vol. 6, no. 6, pp. 1186–1189, 2000.

[20] H. Search, C. Journals, A. Contact, M. Iopscience, and I. P. Address, “Colour centres in germanosilicate glass and o p t i d fibres,” vol. 6901.

[21] O. I. Medvedkov, S. A. Vasiliev, P. I. Gnusin, and E. M. Dianov, “Photosensitivity of optical fibers with extremely high germanium concentration,” *J. Appl. Phys. Appl. Phys. Opt. Mater. EXPRESS 1478 Exp. Tech*, vol. 35, no. 19, pp. 1085–1103, 2005.

[22] J. Stone, “Photorefractivity in GeO2-doped silica fibers,” *J. Appl. Phys.*, vol. 62, no. 11, p. 4371, Dec. 1987.

[23] K. O. Hill, Y. Fujii, D. C. Johnson, and B. S. Kawasaki, “Photosensitivity in optical fiber waveguides: Application to reflection filter fabrication,” *Appl. Phys. Lett.*, vol. 32, no. 10, p. 647, Aug. 1978.

[24] “SELF-POWERED FIBER BRAGG GRATING SENSORS by Benjamin W . McMillen B . S . Electrical Engineering , University of Pittsburgh 2003 Submitted to the Graduate

Faculty of The School of Engineering in partial fulfillment of the requirements for the degree of Ma," 2007.

[25] G. Meltz, W. W. Morey, and W. H. Glenn, "Formation of Bragg gratings in optical fibers by a transverse holographic method.," *Opt. Lett.*, vol. 14, no. 15, pp. 823–825, 1989.

[26] D. L. Williams, S. T. Davey, R. Kashyap, J. R. Armitage, and B. J. Ainslie, "Direct observation of UV induced bleaching of 240 nm absorption band in photosensitive germanosilicate glass fibres," *Electron. Lett. (ISSN 0013-5194), vol. 28, Feb. 13, 1992, p. 369-371.*, vol. 28, pp. 369–371, 1992.

[27] K. T. V. Grattan and B. T. Meggitt, *Optical Fiber Sensor Technology Advanced Applications - Bragg Gratings and Distributed Sensors*. Springer US, 2000.

[28] H. Hosono, Y. Abe, D. L. Kinser, R. a Weeks, K. Muta, and H. Kawazoe, "Nature and origin of the 5-eV band in SiO$_{2}$:GeO$_{2}$ glasses," *Phys. Rev. B*, vol. 46, no. 18, pp. 11445–11451, 1992.

[29] et al. Dong, Liang, "study of UV absorption in germanosilicate fiber preforms," in *Conference on Lasers and Electro-Optics. Vol. 8. Optical Society of America*, 1994.

[30] S. Pal, J. Mandal, T. Sun, and K. T. V Grattan, "Analysis of thermal decay and prediction of operational lifetime for a type I boron-germanium codoped fiber Bragg grating.," *Appl. Opt.*, vol. 42, no. 12, pp. 2188–97, 2003.

[31] E. Li, X. Wang, and C. Zhang, "Fiber-optic temperature sensor based on interference of selective higher-order modes," *Appl. Phys. Lett.*, vol. 89, no. 9, pp. 9–12, 2006.

[32] A. D. Kersey, M. A. Davis, H. J. Patrick, M. LeBlanc, K. P. Koo, C. G. Askins, M. A. Putnam, and E. J. Friebele, "Fiber grating sensors," *J. Light. Technol.*, vol. 15, no. 8, pp. 1442–1462, 1997.

[33] V. R. Mamidi, S. Kamineni, L. N. S. P. Ravinuthala, S. S. Madhuvarasu, V. R. Thumu, V. R. Pachava, and K. Putha, "Fiber Bragg grating-based high temperature sensor and its low cost interrogation system with enhanced resolution," *Opt. Appl.*, vol. 44, no. 2, pp. 299–308, 2014.

[34] R. W. Fallon, L. Zhang, L. A. Everall, J. A. R. Williams, and I. Bennion, "All-fibre optical sensing system: Bragg grating sensor interrogated by a long-period grating," *Meas. Sci. Technol.*, vol. 9, no. 12, pp. 1969–1973, 1998.

[35] V. R. Mamidi, S. Kamineni, L. N. Sai Prasad Ravinuthala, V. Thumu, and V. R. Pachava, "Method to athermalize a long-period fiber grating for interrogation of fiber Bragg grating–based sensors," *Opt. Eng.*, vol. 53, no. 9, p. 096111, Sep. 2014.

[36] O. Svelto, *Principles of lasers*. London, New York, Rheine: Heyden, 1976.

[37] "What is ASE light source ?-FiberLabs Inc." [Online]. Available: http://www.fiberlabs-inc.com/about ase.htm. [Accessed: 17-May-2016].

[38] D. Kinet, P. Mégret, K. W. Goossen, L. Qiu, D. Heider, and C. Caucheteur, "Fiber Bragg grating sensors toward structural health monitoring in composite materials: challenges and solutions," *Sensors*, vol. 14, no. 4, pp. 7394–7419, 2014.

[39] S. J. Mihailov, "Fiber bragg grating sensors for harsh environments," *Sensors*, vol. 12, no. 2, pp. 1898–1918, 2012.

[40] L. Polz, Q. Nguyen, H. Bartelt, and J. Roths, "Fiber Bragg gratings in hydrogen-loaded photosensitive fiber with two regeneration regimes," *Opt. Commun.*, vol. 313, pp. 128–133, 2013.